ACS APPLIED MATERIALS & INTERFACES

Research Article

www.acsami.org

Dual Drug Conjugated Nanoparticle for Simultaneous Targeting of Mitochondria and Nucleus in Cancer Cells

Abhik Mallick,[†] Piyush More,[†,§] Sougata Ghosh,[§] Rohan Chippalkatti,[§,Φ] Balu A. Chopade,[⊥] Mayurika Lahiri,[Φ] and Sudipta Basu*[,†]

[†]Department of Chemistry, Indian Institute of Science Education and Research (IISER)-Pune, Pune, 411021, Maharashtra India
[§]Institute of Bioinformatics and Biotechnology (IBB), University of Pune, Pune, 411007, Maharashtra India
[Φ]Department of Biology, Indian Institute of Science Education and Research (IISER)-Pune, Pune, 411021, Maharashtra India
[⊥]Department of Microbiology, Savitribai Phule Pune University, Pune, 411007, Maharashtra India

Supporting Information

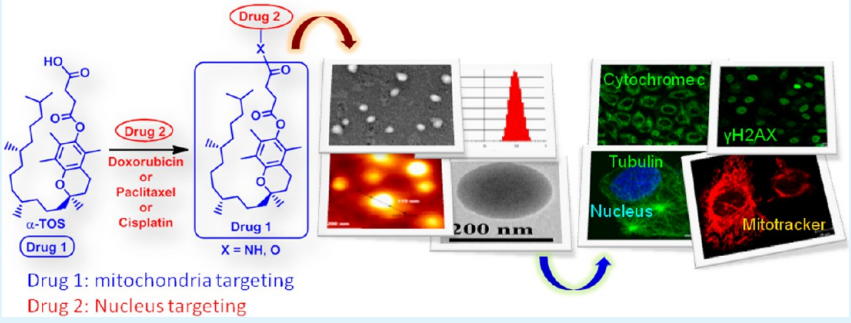

ABSTRACT: Effective targeting of mitochondria has emerged as an alternative strategy in cancer chemotherapy. However, considering mitochondria's crucial role in cellular energetics, metabolism and signaling, targeting mitochondria with small molecules would lead to severe side effects in cancer patients. Moreover, mitochondrial functions are highly dependent on other cellular organelles like nucleus. Hence, simultaneous targeting of mitochondria and nucleus could lead to more effective anticancer strategy. To achieve this goal, we have developed sub 200 nm particles from dual drug conjugates derived from direct tethering of mitochondria damaging drug (α- tocopheryl succinate) and nucleus damaging drugs (cisplatin, doxorubicin and paclitaxel). These dual drug conjugated nanoparticles were internalized into the acidic lysosomal compartments of the HeLa cervical cancer cells through endocytosis and induced apoptosis through cell cycle arrest. These nanoparticles damaged mitochondrial morphology and triggered the release of cytochrome c. Furthermore, these nanoparticles target nucleus to induce DNA damage, fragment the nuclear morphology and damage the cytoskeletal protein tubulin. Therefore, these dual drug conjugated nanoparticles can be successfully used as a platform technology for simultaneous targeting of multiple subcellular organelles in cancer cells to improve the therapeutic efficacy of the free drugs.

KEYWORDS: *mitochondria, nucleus, dual drug conjugated nanoparticle, cancer, tocopheryl succinate, cisplatin, doxorubicin, paclitaxel*

1. INTRODUCTION

Cancer is the second leading cause of death globally having 8.2 million deaths and 14.1 million new cases in the year 2012.[1,2] Hence, striving toward the elimination and prevention of cancer is one of the most leading challenges in current medical science. Traditional cancer treatment is based on using high cytotoxic drugs or specific kinase inhibitors to target rapid cell division, receptor tyrosine kinases and downstream signaling, respectively.[3] However, most tumors can escape single drug treatment by developing drug resistance through intrinsic or extrinsic mechanisms.[4,5] Hence, modern cancer treatment relies on using drug combinations to inhibit multiple targets, maximize therapeutic outcomes and overcome drug resistance.[6,7] In recent years, mitochondrion has emerged as an important alternative target in cancer therapeutics due to its diverse functions including cellular energy production by generating ATP via respiration, regulating danger signaling and containing mitochondrial DNA (mtDNA) as genomic material.[8,9] As a result, routing the DNA damaging drugs and kinase inhibitors specifically into mitochondria by tagging mitochondria targeting peptides or triphenylphosphine (TPP) moiety has become an alternative strategy in cancer therapeutics.[10−13] Recently, Lippard and co-workers developed mitaplatin and vitamin E analogues-Pt(IV) complexes as prodrugs for simultaneous targeting of nuclear DNA and mitochondria.[14,15] However, targeting mitochondrial function

Received: December 24, 2014
Accepted: March 26, 2015
Published: March 26, 2015

DOI: 10.1021/am5090226
ACS Appl. Mater. Interfaces 2015, 7, 7584−7598

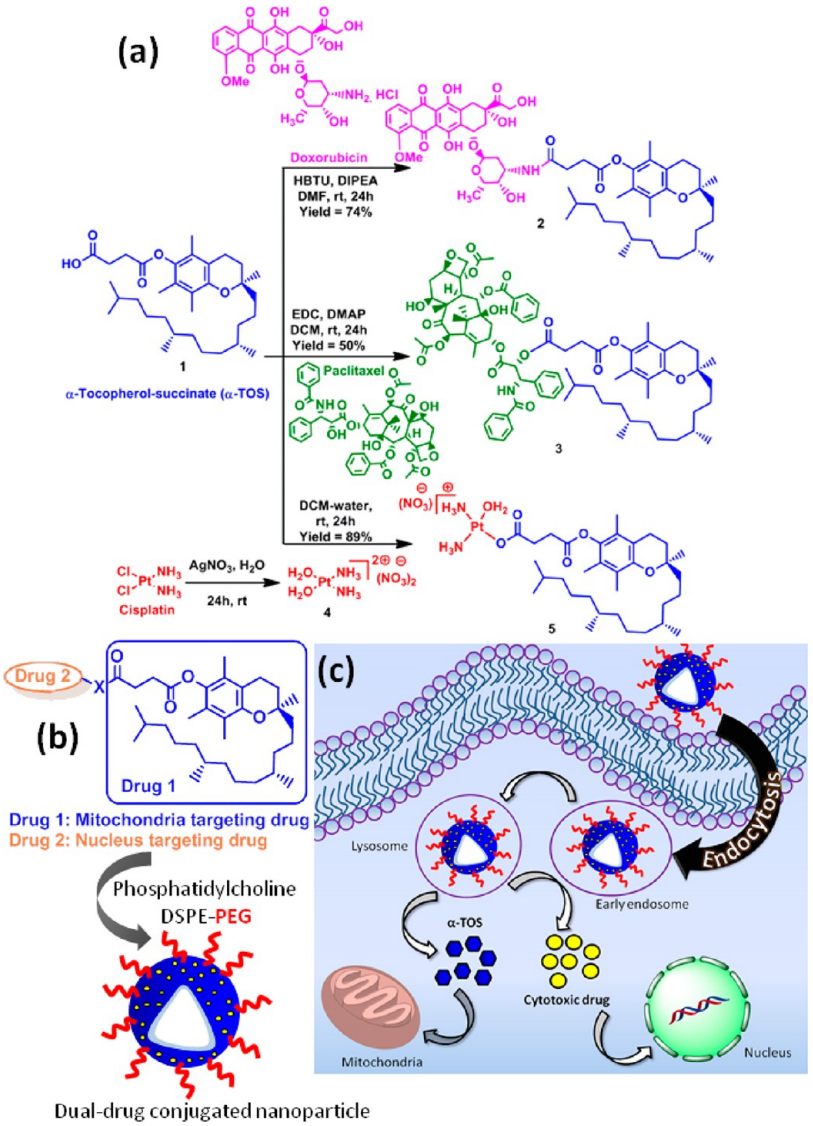

Figure 1. Schematic diagram of dual drug conjugate synthesis, nanoparticle engineering and cellular internalization. (a) Synthesis of dual drug conjugates from α-TOS and doxorubicin, paclitaxel and cisplatin by amide, ester and covalent coordinate conjugation, respectively. (b) Schematic representation of dual drug conjugated nanoparticle synthesis by using phosphatidylcholine (PC) and DSPE-PEG. (c) Schematic diagram of internalization of dual drug conjugated nanoparticle into lysosomal compartment through endocytosis and target mitochondria and nucleus.

by small molecule drugs would lead to severe side effects to the cancer patients considering mitochondria's critical role in governing cellular metabolism in healthy cells, as well as diverse interconnected functions like autophagy and apoptosis.[16,17]

Nanotechnology based platforms have revolutionized cancer therapeutics in past decade by delivering small molecule drugs, siRNAs and therapeutic proteins specifically into tumors by using unique enhanced permeability and retention (EPR) effect or cancer biomarker driven active targeting.[18−21] The nanovectors having size <200 nm were found to be most effective in cancer therapy and diagnosis due to their preferential accumulation into tumor tissues compared to the healthy tissues.[22] Several nanovectors including polymeric nanoparticles,[23−25] nanocell,[26] layer-by-layer nanoparticles,[27] graphene oxide,[28] gel-liposome,[29] and carbon nanotubes[30] have been explored for effective dual drug delivery in cancer tissues to reduce the toxic side effects. However, nanoparticle mediated delivery of drugs to the specific subcellular compartments or organelles remains elusive because of the similarity in the structure and function of the organelles between healthy cells and cancer cells. Moreover, nanoparticle mediated selective targeting of organelles in cancer cells would lead to minimize the off-target toxicity in the healthy cells as well as overcome drug resistance. Recently, Dhar and co-workers developed TPP coated biocompatible PLGA−PEG-based blended nanoparticles and gold nanoparticles to deliver different drugs selectively to mitochondria.[31,32] Although, specific targeting of mitochondria emerged as an interesting strategy to alter the bioenergetics of cancer cells, mitochondria depend on the nucleus and other cellular organelles for most of their proteins and lipids, as well as their cellular functions.[33,34] Moreover, nucleus is the most important cellular organelle, containing genomic materials (nuclear DNA, RNA, and chromosomes) and regulates important functions like transcription, cell cycle and cell division in healthy cells as well as in cancer cells.[35]

We hypothesize that dual drug conjugated nanoparticles would preferentially extravasate into tumor tissue through EPR effect and mediate simultaneous subcellular targeting of

DOI: 10.1021/am5090226
ACS Appl. Mater. Interfaces 2015, 7, 7584−7598

mitochondria and nucleus leading to more effective therapeutics in cancer. Aiming at this goal, we have chosen α-tocopheryl succinate (α-TOS) as mitochondria targeting drug, cisplatin and doxorubicin as different clinically approved nuclear DNA damaging drugs and paclitaxel as microtubule binding drug to disrupt the shape of the cellular nucleus. α-TOS is a redox silent analogue of vitamin E, which induces apoptosis in different types of cancers including prostate, breast, lung, colon, cervical, endometrial, as well as hematopoietic cancers,[36−38] by targeting the mitochondrial complex II and causing conformational changes in the pro-apoptotic protein Bak, leading to permeabilization of mitochondrial outer membrane (MOM) and subsequent production of cytochrome c.[39−41] Moreover, α-TOS showed improved therapeutic efficacy in combination with cisplatin,[42] doxorubicin,[43] and paclitaxel.[44] Although α-TOS shows broad antitumor effect without any toxicity to normal tissues,[45,46] cisplatin, doxorubicin, and paclitaxel show dose-dependent nephrotoxicity, cardiotoxicity, and neurotoxicity, respectively, to the patients.[47−49]

As a proof of concept, in this manuscript, we have directly conjugated α-TOS with cisplatin, doxorubicin, and paclitaxel without any additional linker (Figure 1a). We engineered sub 200 nm particles from these dual drug conjugates, which were endocytosed into the acidic lysosomal compartments of HeLa cervical cancer cells temporally and released the dual drugs in a slow and sustained manner to target mitochondria and nucleus simultaneously (Figure 1b and Figure 1c). These dual drug conjugated nanoparticles showed cytotoxicity by inducing apoptosis through damaging mitochondrial outer membrane (MOM) to release cytochome c, as well as damaging nuclear DNA and tubulin to arrest the cell cycle. These dual drug conjugated nanoparticles have potential to simultaneous targeting of multiple subcellular organelles to escalate the therapeutic outcomes in modern cancer treatment.

2. MATERIALS AND METHODS

2.1. Material. All reactions were performed under inert conditions unless otherwise indicated. All commercially obtained compounds were used without further purification. Ethyl acetate, petroleum ether, dry dichloromethane (DCM), methanol, dry dimethylformamide (DMF), alpha-tocopherol succinate, silver nitrate, sodium sulfate, sodium chloride, *o*-phenylenediamine, *N*-(3-(dimethylamino)propyl)-*N*′-ethylcarbodiimide hydrochloride (EDC), *O*-(benzotriazol-1-yl)-*N*,*N*,*N*′,*N*′-tetramethyluronium hexafluorophosphate (HBTU), *N*,*N*-dimethyl amino pyridine (DMAP), hydrochloric acid, chloroform-*d* ($CDCl_3$), dimethyl sulfoxide (DMSO-*d6*), double distilled water, diisopropyl ethylamine (DIPEA), L-phosphatidylcholine, sephadex G-25, sodium dodecyl sulfate (SDS), paraformaldehyde, *n*-propyl gallate, glycerol, Triton X-100, ethyl alcohol, and silicon wafer for FE-SEM were bought from Sigma-Aldrich. Paclitaxel, cisplatin, and doxorubicin were bought from Selleck Chemicals. 1,2-Distearoyl-*sn*-Glycero-3-phosphoethanolamine-*N*-[amino(polythylene glycol)2000] (DSPE-PEG) and the mini hand-held extruder kit (including 0.2 nm Whatman Nucleopore Track-Etch Membrane, whatman filter supports, and 1.0 mL Hamiltonian syringes) were bought from Avanti PolarLipids, Inc. Analytical thin-layer chromatography (TLC) was performed using precoated silica gel aluminum sheets 60 F254 bought from EMD Laboratories. DMEM media and 3-(4, 5-dimethylthiazol-2-yl)-2,5-diphenyltetrazolium bromide (MTT), propidium iodide, RNase, $MgCl_2$, and DAPI were purchased from HiMedia. 96-well plates, 6-well plates, 15 and 50 mL graduated sterile centrifuge tubes and tissue culture flasks with filter cap sterile were purchased from Tarsons Product Pvt. Ltd. Annexin-V-FLUOS Staining Kit was purchased from Roche. LysoSensor Green DND-153, LysoTracker Green DND-26, MitoTracker Red CMXRos, Alexa Fluor Fluorescent Streptavidin Conjugate, *SlowFade* Gold Antifade Reagent, and caspase-3, -8, and -9 protease assay kits were obtained from Life Technologies. Cytochrome c rabbit mAb, antirabbit IgG and HRP-linked antibody were obtained from CST. Anti-PARP antibody-clone 7A10, anti-phospho-histone H2AX (Ser139) antibody-clone JBW301, GAPDH antibody, goat antimouse IgG antibody, (H + L) HRP conjugate and rabbit antichicken IgG antibody. HRP conjugates were obtained from Merck Millipore. Alexa Fluor 488 goat antimouse IgG (H + L) antibody and alexa fluor 488 goat antirabbit IgG (H + L) antibody were purchased from Life technologies. HeLa and HEK293 cells were obtained from National Centre for Cell Science (NCCS), Pune. Spots on the TLC plates were visualized using alkanine permanganate or phosphomolybdic acid hydrate in methanol. ^1H (400 MHz) spectra were obtained on a Jeol-400 spectrophotometer. The chemical shifts are expressed in parts per million (ppm) using suitable deuterated NMR solvents with reference to TMS at 0 ppm. The release kinetic data, drug loading, nanoparticle size and cell viability assay were plotted using GraphPad Prism software. The laser scanning confocal microscopy was performed by Zeiss LSM 710 machine. Each sample was done in triplicate. FACS analysis was performed using BD FACS Calibur flow cytometer.

2.2. Synthesis of α-Tocopherol Succinate-Doxorubicin Conjugate (2). α-Tocopherol succinate (5 mg, 0.009 mmol, 1 equiv) was dissolved in 1 mL dry DMF. After continuous stirring under inert condition at 0 °C for 5 min, HBTU (15 mg, 0.014 mmol, 1.5 equiv) was added followed by addition of DIPEA (6 μL, 0.037 mmol, 4 equiv). The reaction mixture was cooled down for 10 min at 0 °C and doxorubicin (6.55 mg, 0.011 mmol, 1.2 equiv) was added to it. The reaction was stirred at room temperature for 24 h. The reaction was then quenched with 0.1 N HCl (10 mL) and H_2O (40 mL). The organic layer was extracted with DCM (2 × 20 mL). To remove dissolved salts present in the reaction mixture, wash with brine solution was given (2 × 30 mL). Anhydrous sodium sulfate (Na_2SO_4) was added to the organic layer to remove the trace amount of water present. Organic layer was then concentrated using rotary evaporator. Crude product was purified by silica gel (100−200 mesh size) column chromatography by using 1% methanol in DCM to obtain product as a red colored solid. **Yield:** 7.4 mg (74.34%).

2.3. Synthesis of α-Tocopherol Succinate-Paclitaxel Conjugate (3). α-Tocopherol succinate (**1**) (2.5 mg, 0.0047 mmol, 1 equiv) was dissolved in 1 mL dry dichloromethane (DCM) under inert atmosphere and cooled to 0 °C. Subsequently, *N*-(3-dimethylaminopropyl)-*N*′-ethylcarbodiimide hydrochloride (EDC) (0.99 mg, 0.005 mmol, 1.1 equiv), diisopropylethylamine (DIPEA) (2.4 μL, 0.014 mmol, 3 equiv), and 4-(dimethylamino) pyridine (DMAP) (0.06 mg, 0.00047 mmol, 0.1 equiv) were added to the reaction mixture with continuous stirring under inert condition. After 30 min, paclitaxel (4.33 mg, 0.005 mmol, 1.1 equiv) was added into the reaction mixture. The reaction was monitored by TLC. After 24 h, the reaction was quenched with 0.1 N HCl (1 mL), water (5 mL), and diluted with DCM (10 mL). The organic layer was extracted with DCM (2 × 15 mL) and washed with brine solution (10 mL). The organic layer was dried over anhydrous sodium sulfate (Na_2SO_4). Organic solvent was then evaporated using rotary evaporator and the crude product was purified using silica gel (100−200 mesh size) column chromatography with 30% ethyl acetate in petroleum ether to obtain the pure compound. Yield: 3 mg (50.14%).

2.4. Synthesis of Aquated Cisplatin (4). Fifty milligrams of cisplatin was dissolved in 10 mL of water and 28 mg of silver nitrate was added to the solution. Reaction mixture was then stirred at room temperature under dark conditions for 24 h. Reaction mixture turned milky white and was centrifuged for 15 to 20 min to precipitate silver chloride. The supernatant is then filtered through 0.2 μm filter and compound was obtained for further reaction.

2.5. Synthesis of α-Tocopherol Succinate-Cisplatin Conjugate (5). α-Tocopherol succinate (**1**) (5 mg, 0.009 mmol, 1 equiv) was dissolved in 1 mL of DMF and aquated cisplatin (**4**) (500 μL = 2.5 mg, 0.009 mmol, 1 equiv) was added to it. It was kept for stirring for 24 h. After 24 h, solvent was evaporated by rotary evaporator. Yield: 6.5 mg (89.0%).

DOI: 10.1021/am5090226
ACS Appl. Mater. Interfaces 2015, 7, 7584−7598

2.6. General Procedure of Synthesizing Dual Drug Conjugated Nanoparticles and Rhodamine Loaded Nanoparticles. Ten milligrams of L-α-phosphatidylcholine (PC), 5.0 mg of dual drug conjugates (**2**, **3**, and **5**) and 1 mg of 1,2-distearoyl-*sn*-glycero-3-phosphoethanolamine-*N*-[amino(polythylene glycol)2000] (DSPE-PEG) (1 mg of rhodamine was added for the synthesis of α-TOS-CDDP-Rho-NP and α-TOS-Paclitaxel-Rho-NP) were dissolved in 5.0 mL of DCM. Solvent was evaporated into a thin and uniform film with the help of a rotary evaporator. After thorough drying with vacuum pump dual drug conjugate film was hydrated with 1.0 mL H_2O for 2 h at 60 °C. It was passed though Sephadex G-25 column and extruded through 200 nm Whatmann polycarbonate membrane at 65 °C to obtain sub 200 nm particles. The dual drug conjugated nanoparticles, α-TOS-CDDP-Rho-NP and α-TOS-Paclitaxel-Rho-NP were stored at 4 °C for further use.

2.7. General Procedure for Quantification of Drug Loading. A calibration curve was plotted in the concentration range of 2.5 to 100 μM (for α-TOS), 10−40 μM (for paclitaxel), and 10−100 μM (for doxorubicin) by diluting the 1 mM standard stock solution of drugs in dimethyl sulfoxide (DMSO). The absorbance was measured at 287, 271, and 490 nm for α-TOS, paclitaxel and doxorubicin respectively against the corresponding solvent blank. The linearity was plotted for absorbance (A) against concentration (C). For drug loading in nanoparticles, prepared nanoparticles were dissolved in spectroscopic grade DMSO in 5%, 10% and 15% dilution. Absorbance was measured at characteristic wavelength against the corresponding solvent blank in 200 μL quartz cuvette and from the calibration curve drug loading was measured in triplicate. For the quantification of cisplatin, a different strategy was followed since it is not itself UV active. For the calibration curve, 1 mM stock was prepared by dissolving cisplatin into 1.2 mg/mL solution of o-phenylenediamine in DMF and heated at 100 °C for 4 h, until the solution turned deep green in color. Range of further dilutions from 2.5 μM to 15 μM was obtained by diluting stock solution with DMF. The absorbance was measured at 706 nm (which is characteristic λ_{max} for cisplatin) against DMF as blank. Linear relationship was obtained by plotting the absorbance values (A) against corresponding concentrations (C). For drug loading in nanoparticles, prepared nanoparticles (100 μL) were dissolved in 500 μL o-phenylenediamine (1.2 mg/mL of spectroscopic grade DMF). Then it was heated at 100 °C for 4 h until greenish yellow color appears. From the stock of the greenish yellow solution, 5%, 10%, 15% dilutions were prepared. Absorbance was measured at characteristic wavelength against the corresponding solvent blank in 200 μL quartz cuvette and from the calibration curve drug loading was measured in triplicate in the similar way as the above.

2.8. Determination of Size Distribution of Nanoparticles by Dynamic Light Scattering (DLS). The mean particle size of the dual drug conjugated nanoparticles was measured by dynamic light scattering (DLS) method using Zetasizer Nano2590 (Malvern, UK). 50 μL of nanoparticle solution was diluted to 1 mL using DI water and 3 sets of 10 measurements each were performed at 90° scattering angle to get the average particle size.

2.9. Field-Emission Scanning Electron Microscopy (FESEM) of Dual Drug Conjugated Nanoparticles. Five microliters of dual-drug conjugated nanoparticles in water was placed on a silicon chip without any dopant, and it was allowed to dry at room temperature under vacuum desiccators for 2 h. The silicon chip was then gold coated (30−40 nm thickness) using Quorum, Q150T-E5. The FESEM measurements were done using Carl Zeiss, Ultra plus, scanning electron microscope at an operating voltage of 4.0 kV.

2.10. Atomic Force Microscopy (AFM) of Dual Drug Conjugated Nanoparticles. Five microliters of dual drug conjugated nanoparticles in water was placed on mica sheet and dried under the vacuum desiccators for 2 h. Shape and size of dual-drug conjugated nanoparticles were determined using NanoWizard Atomic Force Microscopy (AFM).

2.11. Transmission Electron Microscopy (TEM) of Dual Drug Conjugated Nanoparticles. Fifteen microliters of nanoparticles in water was placed on a TEM copper grid. After 30 min, this sample drop was wicked off by using filter paper and then 15 μL of freshly prepared 0.25% uranyl acetate (2.5 mg uranyl acetate in 1 mL dd water) solution was placed on the TEM copper grid. After 1 min, uranyl acetate solution was wicked off and the sample was washed three times with 15 μL of dd water each time. The sample was dried overnight on a clean dust free surface under a funnel. The dual drug conjugated nanoparticles were imaged using Tecnai T300 HR-TEM and Tecnai G2 20-Twin LR-TEM instruments.

2.12. Stability of the Nanoparticles at 4 and 37 °C by Dynamic Light Scattering (DLS). The stability of the nanoparticles was checked at 4 and 37 °C by Dynamic Light Scattering method using Zetasizer Nano2590 (Malvern, UK). 200 μL of nanoparticles solution was diluted to 1 mL using DI water and 3 sets of 10 measurements each were performed at 90 scattering angle to get the average particle size. This was done for 14 days keeping the nanoparticles at 4 °C (refrigerator) and 37 °C (incubator) to check its stability at shelf (for storage purpose) as well as in blood circulation temperature. Similarly, the nanoparticles were incubated in DMEM cell culture media containing 10% FBS (or in PBS) at 37 °C for 3 days and size and PDI values were measured in predetermined time points.

2.13. General Procedure for Determining the Drug Release Profile. Concentrated 250 μL of dual drug conjugated nanoparticles were suspended in 250 μL pH = 5.5 solution (or pH = 7.4 solution) and sealed in a dialysis membrane (MWCO = 2000 Da for cisplatin, paclitaxel and doxorubicin release). The dialysis bags were incubated in 10 mL pH = 5.5 solution (or pH = 7.4 solution) at room temperature with gentle shaking. A 400 μL portion of the aliquot was collected from the incubation medium at predetermined time intervals and the released dual drugs were quantified by UV−vis spectrophotometer.

2.14. Cell Viability Assay. Five thousand cells (HeLa and HEK293 cells) were seeded per well in 96-well microtiter plate and incubated overnight in a 5% CO_2 incubator at 37 °C for attachment. Cells were then treated with dual drug conjugated nanoparticles and free drug combinations in different concentrations (0.1, 0.2, 0.4, 0.8, 1.6, 3.2, 6.4, 12.5, 25, 50 μM) for 48 h. Free drugs were dissolved in DMSO to make a stock solution of 5 mM concentration. Serial dilutions of free drugs in DMSO were made from this stock solution and 2 μL of each free drug solution was added to cells to obtain desired final concentrations. Twenty μL of MTT reagent (5 mg/mL) was added to each well and incubated for 4 h at 37 °C. Formazan crystals were then solubilized in 100 μL of the solubilization buffer (10% SDS in 0.01 M HCl) and incubated overnight. Absorbance was measured with spectrophotometer at 550 nm. The percent cell viability was calculated considering the untreated cells as 100% viability and the effectiveness of dual-drug conjugated nanoparticles was compared with the free drug combinations.

2.15. FACS Analysis for Apoptosis Detection. For apoptosis detection, 2×10^6 HeLa cells were incubated in 6-well plates overnight for attachment and then treated with nanoparticles for 24 h at their respective IC_{50} values. After the treatment, media was removed and cells were trypsinized and washed twice with PBS by means of centrifugation at 750 rpm for 4 min. Cell pellet was then resuspended in 100 μL of Annexin-V-FLUOS labeling solution (Annexin-V-FLUOS Staining Kit from Roche) and incubated in 500 μL of incubation buffer at 25 °C for 15 min. Cells were then passed through cell strainer to get uniform cell suspension and analyzed using BD FACS Calibur to detect the apoptosis.

2.16. Caspase Activity Assay. Caspase activities for caspase-3, caspase-8, and caspase-9 were assayed using Caspase-3, 8, and 9 colorimetric protease assay kit from Life Technologies. Caspase-3, caspase-8 and caspase-9 recognize the amino acid sequence, DEVD (Asp-Glue-Val-Asp), IETD (Ile-Glu-Thr-Asp), and LEHD (Leu-Glu-His-Asp), respectively. After treating the HeLa cells with dual drug conjugated nanoparticles for 24 h, 3×10^6 cells were centrifuged and resuspended in 50 μL chilled cell lysis buffer and incubated in ice for 10 min. Cell lysates were then centrifuged at 10,000*g* for 1 min and supernatant was collected for assaying the caspase activities. Total protein concentration was estimated using protein estimation kit by bradford protein assay (GeNei Merck) and cytosol extracts were diluted to a concentration of 50 μg protein per 50 μL of cell lysis

DOI: 10.1021/am5090226
ACS Appl. Mater. Interfaces 2015, 7, 7584−7598

buffer. 50 μL of 2× reaction buffer was added to each 50 μL sample followed by addition of 5 μL substrate specific for each caspase and incubated at 37 °C in dark for 2 h. Substrates consist of a chromophore, *p*-nitroanilide (*p*NA) and the amino acid sequence of the respective caspase cleavage site. Upon proteolytic cleavage of substrate by caspase, generated free *p*NA was measured spectrophotometrically at 405 nm. Fold increase in caspase activity was calculated by direct comparison to the level of control absorbance.

2.17. Cell Cycle Analysis. Two $\times 10^6$ HeLa cells were seeded in a 6 well plate and allowed to attach overnight in a 5% CO_2 incubator at 37 °C. Cells were treated with dual drug conjugated nanoparticles at a concentration corresponding to the IC_{50} value of respective drugs for 24 h. After the treatment, the cells were harvested and washed with 1 mL PBS (pH = 7.4) and then centrifuged at 850 rpm for 4 min. Supernatant was discarded and cells were fixed in 70% ice-chilled ethyl alcohol for 30 min at −20 °C. Fixed cells were centrifuged at 850 rpm for 4 min. Fixing solution was aspirated and 1 mL ice-chilled PBS was added. Cells were again centrifuged at 850 rpm for 4 min and resuspended in 0.5 mL of the staining solution (50 μL of 1 mg mL^{-1} propidium iodide, 50 μL of 1 mg mL^{-1} RNase and 400 μL PBS). Cells were then analyzed using BD Accuri C6 flow cytometer.

2.18. Confocal Laser Scanning Microscopy (CLSM) Studies. *2.18.1. Cellular Internalization.* Five $\times 10^4$ HeLa cells were seeded on a coverslip in a 6 well plate and incubated overnight in a 5% CO_2 incubator at 37 °C for attachment. Cells were then first washed with PBS (pH = 7.4) and then treated with α-TOS-Dox-NP (at a concentration equivalent to 2 μg mL^{-1} of doxorubicin) and free doxorubicin (2 μg mL^{-1}) for 1, 3, and 6 h. Cells were then washed twice with PBS and fixed with 500 μL of paraformaldehyde (3.7% in PBS, pH = 6.9) by incubating for 10 min at 4 °C. The paraformaldehyde was aspirated and cells are washed trice with PBS. Low pH lysosomes were stained with 50 nM LysoTracker Green DND-26 (Invitrogen) by incubating the cells at 37 °C for 45 min. The cells were then washed three times to remove the unbound LysoTracker Green DND-26 followed by staining the cells for nuclei with 2 μg mL^{-1} DAPI (HiMedia) by incubating at 37 °C for 20 min. Then cells were washed three times with PBS and mounted on a glass slide using 5 μL *SlowFade* Gold Antifade Reagent. The slides were subjected to fluorescence imaging using a CLSM (Zeiss LSM 710).

2.18.2. Mitochondrial Imaging. Five $\times 10^4$ HeLa cells were seeded on a coverslip in a 6 well plate and incubated overnight in a 5% CO_2 incubator at 37 °C for attachment. Cells were then treated with dual drug conjugated nanoparticles at a concentration corresponding to the IC_{50} value of respective drugs for 24 h. Cells were then washed twice with PBS (pH = 7.4) and treated with MitoTracker Red CMXROS at a concentration of 200 nM in PBS and incubated in dark at 37 °C for 25 min. Staining solution was aspirated and cells are washed thrice with PBS and then fixed with 3.7% paraformaldehyde at 37 °C for 15 min. Fixing solution was discarded and cells are permeabilized with PBS containing 0.2% TritonX. 200 μL of Alexa Fluor 488 streptavidin conjugate (2 μg mL^{-1}) was added to the cells and incubated for 90 min at 37 °C in dark. Cells were washed thrice with PBS and mounted on a glass slide using *SlowFade* gold antifade reagent. The slides were subjected to fluorescence imaging using a CLSM (Zeiss LSM 710).

2.18.3. General Procedure for Immunostaining to Visualize Cytochrome c, γH2AX, PARP, and Tubulin. Five $\times 10^4$ HeLa cells were seeded on a coverslip in a 6 well plate and incubated overnight in a 5% CO_2 incubator at 37 °C for attachment. Cells were then treated with dual drug conjugated nanoparticles at corresponding IC_{50} concentration for 24 h. Cells were washed once with PBS and then fixed with 3.7% paraformaldehyde at 37 °C for 15 min. Cells were then washed twice with PBS (pH = 7.4) and were permeabilized by incubating in blocking buffer (PBS containing 0.3% tween and 5% FBS) at room temperature. Cells were then incubated in primary antibody solution (cytochrome c, γH2AX, PARP in 1:100 dilution and tubulin in 1:2500 dilutions) at 37 °C for 3 h. Cells are washed thrice with blocking buffer. Then cells were incubated in fluorochrome conjugated secondary antibody solution (1:500 dilution) at 37 °C for 40 min in dark. Cells were washed thrice with PBS and mounted on a glass slide using SlowFade gold antifade reagent. The slides were subjected to fluorescence imaging using a CLSM (Zeiss LSM 710).

2.19. General Procedure for Western Blot Analysis. After 24 h of dual drug conjugated nanoparticle treatment in their corresponding IC_{50} concentrations, HeLa cells were lysed and suspended in sample buffer. Proteins were separated using SDS-polyacrylamide gel electrophoresis (SDS-PAGE) and then proteins were transferred onto the membrane (electroblotting). Blotted membrane was then blocked in freshly prepared TBS containing nonfat dry milk (5%) for 1 h with constant agitation at room temperature. Membrane was then rinsed once with TBST and then incubated in the primary antibody solution (1:1000 dilution, except 1:2500 gor GAPDH) overnight at 4 °C with gentle agitation (except 4 h for GAPDH). Membrane was then washed 3 times (15 min each) with TBST and then incubated in HRP conjugated secondary antibody solution (1:500 dilution) for 45 min at room temperature with gentle agitation. Membrane was again washed thrice with TBST (5 min each). Protein detection was then followed by using Immobilon Western Chemiluminescent HRP Substrate (membrane was incubated in the substrate for 1 min). Images were acquired using GE Healthcare Lifesciences ImageQuant LAS 4000. After the acquisition, membrane was boiled in distilled water for 5 min and again was reprobed for GAPDH gene. Further image processing and intensity calculations were performed using ImageJ software.

3. RESULTS AND DISCUSSION

3.1. Synthesis and Characterization of Dual Drug Conjugated Nanoparticles. *3.1.1. Synthesis of Dual Drug Conjugates.* The free carboxylic acid group of α-TOS (**1**) was directly conjugated with doxorubicin through amide linkage by using HBTU as coupling agent and DIPEA as base to obtain α-TOS-dox conjugate (**2**, Figure 1a) in 74% yield. α-TOS was conjugated through ester linkage with 2′-OH group of paclitaxel by using EDC as coupling agent and DIPEA as base in the presence of DMAP as catalyst to obtain α-TOS-paclitaxel conjugate (**3**) in 50% yield. Finally, cisplatin (CDDP) was reacted with $AgNO_3$ to generate aquated *cis*-Pt-$[(NH_3)_2(OH_2)_2]^{2+}$ (**4**)[50] which was further conjugated with α-TOS in 1:1 molar ratio by a monocarboxylato bond[51] to synthesize α-TOS-cisplatin conjugate (**5**) in 89% yield. The chemical structures of **2**, **3** and **5** were characterized by ^1H, ^{13}C nuclear magnetic resonance spectroscopy (NMR), high-resolution mass spectroscopy (HR-MS) and MALDI-TOF (Figure S1−S10 in Supporting Information). Moreover, compound **5** showed characteristic monocarboxylato O−Pt peak at −1502 ppm in ^{195}Pt NMR spectroscopy (Figure S11 in Supporting Information).[52]

3.1.2. Engineering of Dual Drug Conjugated Nanoparticles. We engineered nanoparticles from α-TOS-drug conjugates (**2**, **3**, and **5**) by mixing it with phosphatidylcholine (PC) and 1,2-distearoyl-*sn*-glycero-3-phosphoethanolamine-*N*-[amino(polyethylene glycol)-2000] (DSPE-PEG) in 1:2:0.2 weight ratio using a lipid-film hydration method (Figure 1b).[53,54] We chose PC as it is biocompatible, biodegradable and a component of cell membrane. The nanoparticles were provided "stealth" capability by using DSPE-PEG to reduce opsonisation[55] and clearance by reticuloendothelial system (RES). Mean drug loading in different dual drug conjugated nanoparticles was determined by UV−vis spectroscopy to be =2677.1 μg/mL (α-TOS) and 217.7 μg/mL (cisplatin) in α-TOS-CDDP-NP; 2116.2 μg/mL (α-TOS) and 291.4 μg/mL (doxorubicin) in α-TOS-Dox-NP; 784.3 μg/mL (α-TOS) and 84.2 μg/mL (n = 3) (paclitaxel) in α-TOS-Paclitaxel-NP (Figure S12 in Supporting Information), from a concentration vs absorbance calibration graph at characteristic λ_{max} = 480 nm,

DOI: 10.1021/am5090226
ACS Appl. Mater. Interfaces 2015, 7, 7584−7598

271 nm, 706 and 287 nm for doxorubicin, paclitaxel, cisplatin and α-TOS respectively (Figure S13 in Supporting Information). The mean hydrodynamic diameter of the dual drug conjugated nanoparticles were found to be =163.3 nm, 186.3, and 167.9 nm (n = 3) having mean polydispersity index (PDI) = 0.152, 0.154, and 0.199 (n = 3) for α-TOS-Dox-NP, α-TOS-CDDP-NP, and α-TOS-Paclitaxel-NP respectively by dynamic light scattering (DLS) (Figure S14 in Supporting Information). The size, shape and morphology of the dual drug conjugated nanoparticle were characterized by field emission scanning electron microscopy (FESEM, Figure 2a-c), transmission

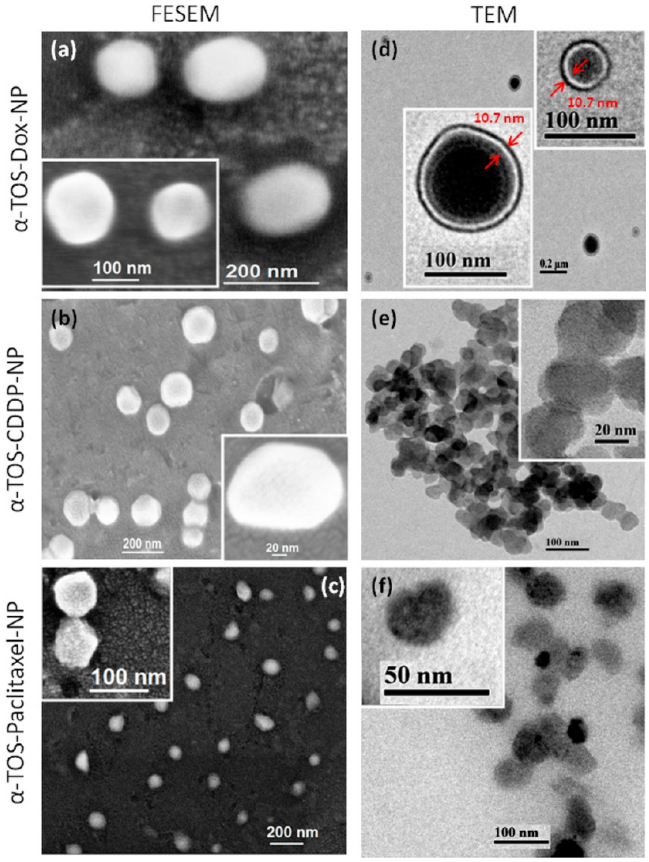

Figure 2. Characterization of dual drug conjugated nanoparticles by electron microscopy. (a–c) FESEM images of α-TOS-Dox-NP, α-TOS-CDDP-NP, and α-TOS-Paclitaxel-NP respectively. (d–f) TEM images of α-TOS-Dox-NP, α-TOS-CDDP-NP, and α-TOS-Paclitaxel-NP respectively.

electron microscopy (TEM, Figure 2d-f) and atomic force microscopy (AFM, Figure S15 in Supporting Information). DLS, FESEM, TEM and AFM data clearly demonstrated the dual drug conjugated nanoparticles were spherical in shape, having sub-200-nm diameter with a membrane thickness ∼10 nm, which is suitable to accumulate into the tumor by EPR effect. Moreover, we confirmed the presence of Pt metal content in α-TOS-cisplatin-NP by energy-dispersive X-ray spectroscopy (EDX) measurements (Figure S16 in Supporting Information).

3.1.3. Stability of Dual Drug Conjugated Nanoparticles. To use these dual drug conjugated nanoparticles in clinics, the nanoparticles should be stable for prolonged time at lower temperature storage conditions. We evaluated the stability of different nanoparticles by measuring the hydrodynamic diameter and PDI values at 4 °C for 14 days by using DLS (Figure S17a in Supporting Information). α-TOS-Dox-NP showed change in size from 173.7 ± 0.9 (PDI = 0.152 ± 0.005) to 191.4 ± 5.6 nm (PDI = 0.350 ± 0.005) after 14 days. On the other hand, α-TOS-CDDP-NP demonstrated change in size from 176.3 ± 0.3 (PDI = 0.154 ± 0.008) to 197.6 ± 3.8 nm (PDI = 0.61 ± 0.23) over 14 days. Finally, α-TOS-Paclitaxel-NP increased in size from 185.0 ± 3.0 (PDI = 0.199 ± 0.009) to 175.3 ± 1.7 nm (PDI = 0.275 ± 0.25) in 14 days (mean ± SEM, n = 3). Moreover, to be successful in the clinics, these dual drug conjugated nanoparticles should be stable inside the blood circulation at 37 °C to reach the tumor by EPR effect. Hence, we evaluated the stability of these nanoparticles at 37 °C in water. The hydrodynamic diameter of α-TOS-Dox-NP changed from 133.7 ± 0.7 to 144.1 ± 1.2 nm with a change in PDI value from 0.28 ± 0.04 to 0.47 ± 0.01 over 3 days (Figure S17b in Supporting Information). Similarly, α-TOS-CDDP-NP changed its size from 152.5 ± 2.0 to 140.5 ± 3.4 nm with a change in PDI value from 0.37 ± 0.0 to 0.37 ± 0.01 over 3 days. Finally, α-TOS-Paclitaxel-NP demonstrated minimal change in size from 173.5 ± 2.0 (PDI = 0.11 ± 0.02) to 172.3 ± 2.2 nm (PDI = 0.48 ± 0.06) over 3 days. Further, we evaluated the stability these dual drug conjugated nanoparticles in phosphate buffer saline (PBS) at 37 °C for 3 days. α-TOS-CDDP-NP increased in size from 162.8 ± 1.8 (PDI = 0.28 ± 0.01) to 180.2 ± 2.8 nm (PDI = 0.54 ± 0.05) (Figure S18a in Supporting Information). On the other hand, α-TOS-Dox-NP showed significant size increase from 147.2 ± 1.3 (PDI = 0.15 ± 0.02) to 190.3 ± 1.5 nm (PDI = 0.37 ± 0.05). Finally, α-TOS-Paclitaxel-NP also increased in size from 138.1 ± 1.3 (PDI = 0.14 ± 0.01) to 175.8 ± 5.7 nm (PDI = 0.31 ± 0.01) in PBS at 37 °C. We finally, evaluated the stability of these nanoparticles in complete DMEM cell culture media with 10% fetal bovine serum (FBS) at 37 °C to mimic the blood circulation milieu. α-TOS-CDDP-NP showed a change in size from 152.0 ± 0.9 to 180.9 ± 2.8 nm with change in PDI from 0.51 ± 0.04 to 0.52 ± 0.07 over 48 h (Figure S18b in Supporting Information). Similarly, α-TOS-Dox-NP showed increase in size from 136.9 ± 1.4 to 189.9 ± 1.4 nm with the increase in PDI from 0.26 ± 0.02 to 0.46 ± 0.01 over 48 h. On the other hand, α-TOS-Paclitaxel-NP showed the increment in size from 127.3 ± 0.01 nm to 154.6 ± 3.0 nm with the change in PDI from 0.21 ± 0.01 to 0.31 ± 0.01 over 48 h. However, all three nanoparticles showed considerable amount of aggregation at 72h of incubation in DMEM with 10% FBS at 37 °C indicated by the huge increase in size of 601.8 ± 43.1 (PDI = 0.52 ± 0.07), 425.5 ± 27.0 (PDI = 0.56 ± 0.7), and 381.2 ± 33.1 nm (PDI = 0.47 ± 0.02) for α-TOS-CDDP-NP, α-TOS-Dox-NP, and α-TOS-Paclitaxel-NP, respectively. From the stability data, it was clear that all the nanoparticles were stable over 14 days at 4 °C as storage temperature. The nanoparticles were also stable at 37 °C in water as well as PBS for 3 days. Moreover, all the nanoparticles showed substantial stability in DMEM cell culture media with 10% FBS as blood circulation mimic for 48h, which was adequate to be accumulated into the tumor tissue through EPR effect.

3.1.4. Release of Dual Drugs from Nanoparticles. To be effective in the clinics, the dual drug conjugated nanoparticles should release the dual drugs in a slow and sustained manner over a period of time. We evaluated the release of the drugs by using dialysis method[53] by incubating the nanoparticles in pH = 5.5 solution at 37 °C which mimics the lysosomal compartment in cancer cells.[56] α-TOS-CDDP-NP released 45.9 ± 14.1%

DOI: 10.1021/am5090226
ACS Appl. Mater. Interfaces 2015, 7, 7584–7598

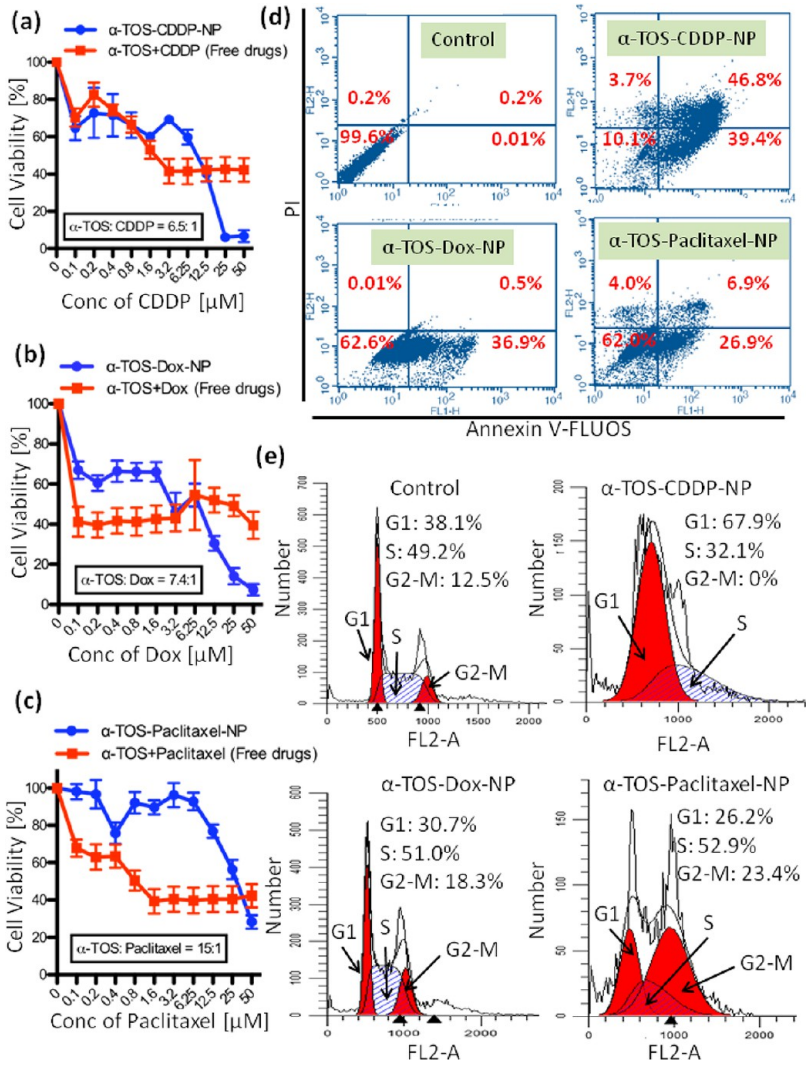

Figure 3. In vitro cytotoxicity assay of dual drug conjugated nanoparticles. (a–c) Dose-dependent cell viability assay of α-TOS-CDDP-NP, α-TOS-Dox-NP, and α-TOS-Paclitaxel-NP respectively in HeLa cells for 48 h. (d) Flow cytometric analysis of apoptosis induced by dual drug conjugated nanoparticles costained by PI and Annexin-V-FLUOS in HeLa cells for 24 h. Lower left: Healthy cells. Lower right: Early apoptotic cells. Upper right: Late apoptotic cells. Upper left: Necrotic cells. The table shows the percentage of cells present in those areas. (e) Cell cycle analysis by staining the DNA in HeLa cells with PI after 24 h post incubation with different dual drug conjugated nanoparticles.

cisplatin and 51.0 ± 5.5% α-TOS at 72 h (Figure S19a in Supporting Information) whereas α-TOS-Dox-NP showed 58.6 ± 6.2% release of α-TOS and only 29.5 ± 4.5% release of doxorubicin at 72 h (Figure S19b in Supporting Information). In the release kinetics experiment, doxorubicin was adsorbed in the dialysis membrane as well as precipitated out from the solution at pH = 5.5, which we suspected to be the reason for lower release of doxorubicin from the nanoparticle (Figure S20a in Supporting Information). We solubilized the precipitate from the dialysis membrane in DMSO and identified it as doxorubicin by UV–vis spectroscopy having characteristic λ_{max} = 480 nm (Figure S20b in Supporting Information). Finally, α-TOS-Paclitaxel-NP demonstrated 78.5 ± 12.6% release of paclitaxel at 72 h and 71.9 ± 21.6% release of α-TOS at 36 h (Figure S19c in Supporting Information). As control experiment, we also incubated the dual drug conjugated nanoparticles in physiological pH of 7.4 and quantified the dual drug release. At pH = 7.4, α-TOS-CDDP-NP released only 24.0 ± 2.4% of cisplatin and 22.1 ± 2.1% of α-TOS at 72 and 48 h, respectively (Figure S19d in Supporting Information), whereas α-TOS-Dox-NP released 15.3 ± 1.0% doxorubicin and 20.9 ± 3.6% α-TOS at 72 h (Figure S19e in Supporting Information). Finally, α-TOS-Paclitaxel-NP also demonstrated 18.8 ± 2.0% and 26.4 ±4.1% release of paclitaxel and α-TOS at 72 h, respectively (Figure S19f in Supporting Information). We rationalized that amide, ester and monocarboxylato linkages in the α-TOS-Dox (**2**), α-TOS-Paclitaxel (**3**), and α-TOS-CDDP (**5**) conjugates respectively are more labile in pH = 5.5 compared to pH = 7.4 which triggered the enhanced dual drug release in acidic pH. We also identified the released free doxorubicin and paclitaxel after acidic hydrolysis from α-TOS-Dox-NP and α-TOS-Paclitaxel-NP respectively by MALDI-TOF experiment (Figure S21a-b in Supporting Information). The release profile data clearly showed higher dual drug release from nanoparticles in a slow and sustained manner over 72 h at pH = 5.5 compared to physiological pH = 7.4. All the data were evaluated as mean ± SEM having n = 3.

3.2. In Vitro Cytotoxicity Assay of Dual Drug Conjugated Nanoparticles. *3.2.1. Cell Viability Assay.* To determine the potential of our dual drug conjugated nano-

DOI: 10.1021/am5090226
ACS Appl. Mater. Interfaces 2015, 7, 7584–7598

particles as cancer therapeutics, we evaluated the *in vitro* efficacy of the nanoparticles in HeLa cervical cancer cell line by cell viability assay. We incubated the HeLa cells with different nanoparticles in a dose dependent manner and evaluated the cell viability by using (3-(4,5-dimethylthiazol-2-yl)-2,5-diphenyl tetrazolium bromide) (MTT) at 48 h post treatment. The α-TOS-CDDP-NP showed IC_{50} = 7.5 μM compared to IC_{50} = 1.7 μM for free cisplatin and α-TOS combination (α-TOS/cisplatin = 6.5:1) (Figure 3a). The α-TOS-CDDP-NP induced 93.9% HeLa cell death compared to 57.7% cell death induced by free cisplatin and α-TOS combination at 25 μM. On the other hand, α-TOS-Dox-NP demonstrated IC_{50} = 6.8 μM compared to IC_{50} = 2.7 μM for the free doxorubicin and α-TOS combination (α-TOS/doxorubicin =7.4:1) (Figure 3b). However, α-TOS-Dox-NP induced 72.6% cell death compared to 60.5% induced by free doxorubicin and α-TOS combination at 50 μM. Finally, α-TOS-Paclitaxel-NP showed IC_{50} = 28.1 μM by inducing 71.7% cell death at 50 μM compared to IC_{50} = 0.8 μM by inducing 57.4% cell death by free paclitaxel and α-TOS combination (α-TOS/paclitaxel =15:1) (Figure 3c). Interestingly, all the different nanoparticles showed improved efficacy in higher doses of drug combinations in contrast to the free drug treatments. We anticipate that different free drug combinations with α-TOS render drug resistance to HeLa cells.[57] However, the exact mechanism needs to be explored. To understand the effect of dual drugs in cytotoxicity in HeLa cells, we used the Chou-Talalay method[58] to determine whether the drug combination effect was synergistic, additive or antagonistic. α-TOS-CDDP-NP and α-TOS-Dox-NP showed combination index (CI) values ranging from 0.05 to 0.62, which clearly indicated the strong synergistic effect (Figure S22 in Supporting Information). However, for α-TOS-Paclitaxel-NP showed CI values varied from 0.4 to 1.08 suggesting additive effect.

We also evaluated the effect of dual drug conjugates in HeLa cells. We incubated the HeLa cells with α-TOS-Dox (**2**), α-TOS-Paclitaxel (**3**) and α-TOS-CDDP (**5**) conjugates in a dose dependent manner and evaluated the cell viability by MTT assay at 48 h postincubation. As controls, we treated the HeLa cells with free cisplatin, doxorubicin, paclitaxel and α-TOS individually. α-TOS-CDDP conjugate (**5**) showed IC_{50} = 9.5 μM (cell viability = 23.0% at 50 μM) compared to IC_{50} = 56 μM (cell viability = 56.1% at 50 μM) and IC_{50} = 63.4 (cell viability = 63.4% at 50 μM) for free cisplatin and free α-TOS respectively (Figure S23a in Supporting Information). Similarly, α-TOS-Dox conjugate (**2**) showed IC_{50} = 7.4 μM (cell viability = 23.1% at 50 μM) compared to IC_{50} = 49 μM (cell viability = 34.6% at 50 μM) for free doxorubicin (Figure S23b in Supporting Information). Finally, α-TOS-Paclitaxel conjugate (**3**) demonstrated IC_{50} = 50 μM (cell viability = 50% at 50 μM) compared to IC_{50} = 25.9 μM (cell viability = 42.2% at 50 μM) for free paclitaxel (Figure S23c in Supporting Information).

To evaluate the side effect of these dual drug conjugated nanoparticles in healthy cells, we treated HEK293 human embryonic kidney cells with different nanoparticles in a dose dependent manner for 24 and 48 h postincubation and quantified the cytotoxicity by MTT assay. At 24h, α-TOS-CDDP-NP showed very high IC_{50} = 63.9 μM compared to IC_{50} = 14.6 μM and IC_{50} = 89.9 μM for free cisplatin and free α-TOS respectively (Figure S24a in Supporting Information). Similarly, α-TOS-Dox-NP also showed high IC_{50} = 56.6 μM compared to IC_{50} = 11 μM for free doxorubicin (Figure S24b in Supporting Information). Finally, α-TOS-Paclitaxel-NP demonstrated IC_{50} = 99.3 μM compared to IC_{50} = 55.4 μM for free paclitaxel (Figure S24c in Supporting Information). However, at 48h, α-TOS-CDDP-NP showed IC_{50} = 6.9 μM compared to IC_{50} = 7.6 μM and IC_{50} = 71.4 μM for free cisplatin and free α-TOS (Figure S24d in Supporting Information). On the other hand, α-TOS-Dox-NP showed IC_{50} = 7.1 μM compared to IC_{50} = 3.3 μM for free doxorubicin (Figure S24e in Supporting Information). Finally, α-TOS-Paclitaxel-NP demonstrated IC_{50} = 29.9 μM compared to IC_{50} = 11.3 μM for free paclitaxel (Figure S24f in Supporting Information).

From these cell viability assays, it was clear that the dual drug conjugated nanoparticles induced enhanced cell death in a dose dependent manner compared to free drug combinations as well as compared to the dual drug conjugates at 48 h. Moreover, the dual drug conjugated nanoparticles showed negligible toxicity to the HEK293 noncancerous embryonic kidney cells at 24 h. However, the dual drug conjugated nanoparticles showed toxicity to the HEK293 cells as 48 h post incubation, we anticipate that the nanoparticles would be homing specifically and selectively into the tumor tissues through the unique leaky vasculature (EPR effect) much earlier than 48 h in *in vivo* milieu. To evaluate the effect of phophatidylcholine (PC) and DSPE-PEG in HeLa cell, we synthesized empty nanoparticles from PC and DSPE-PEG in 2:0.2 ratios in the same lipid film hydration method. We treated the HeLa cells with empty nanoparticle in different concentration and evaluated the cell viability by MTT assay. The empty nanoparticle showed no toxicity in HeLa cells at 1 mg/mL concentration (Figure S25 in Supporting Information).

3.2.2. Apoptosis Assay by FACS. To confirm the potential of the nanoparticles in inducing apoptosis, we used fluorescence activated cell sorting (FACS) method to quantify the amount of cells undergoing apoptosis after treatment compared to the non treated cells. We treated the HeLa cells with different dual drug conjugated nanoparticles for 24h and the cells were labeled with Annexin-V-FLUOS, which binds with externalized phosphatidylserine on the apoptotic cell surface. We further counterstained the cells with propidium iodide (PI) to distinguish between apoptotic and necrotic cells. Indeed, 39% and 47% cells were found in the early and late apoptosis stages respectively with 4% cells in necrotic stage with the treatment of α-TOS-CDDP-NP (Figure 3d). Similarly, 37% and 0.5% cells were found to be in early apoptotic and late apoptotic stages respectively in the treatment with α-TOS-Dox-NP. However, α-TOS-Paclitaxel-NP steered 27% and 7% cells into early and late apoptotic stages, respectively. From this flow cytometric analysis, it was clear that the dual drug conjugated nanoparticles showed cytotoxicity into HeLa cells through induction of apoptosis.

3.2.3. Caspase Assay. Induction of apoptosis in cells leads to the activation of a family of caspases including effector caspase-3 and intitiator caspase-8 and caspase-9.[59−61] We quantified the amount of caspase-3, caspase-8, and caspase-9 as markers of apoptosis by a colorimetric protease assay 24 h of post-treatment with different dual drug conjugated nanoparticles. Amount of caspase-3 was increased 1.1 ± 0.3, 1.7 ± 0.5, and 3.4 ± 1.2 fold for α-TOS-CDDP-NP, α-TOS-Dox-NP, and α-TOS-Paclitaxel-NP, respectively (Figure S26 in Supporting Information). Similarly, caspase-8 activity was also increased to 2.5 ± 0.2, 5.1 ± 1.3 and 1.5 ± 0.1 folds by α-TOS-CDDP-NP, α-TOS-Dox-NP, and α-TOS-Paclitaxel-NP respectively. Finally, caspase-9 activity was increased significantly to 2.8 ± 0.7, 2.9 ± 1.1, and 7.3 ± 0.8 fold by the treatment with α-TOS-CDDP-

DOI: 10.1021/am5090226
ACS Appl. Mater. Interfaces 2015, 7, 7584−7598

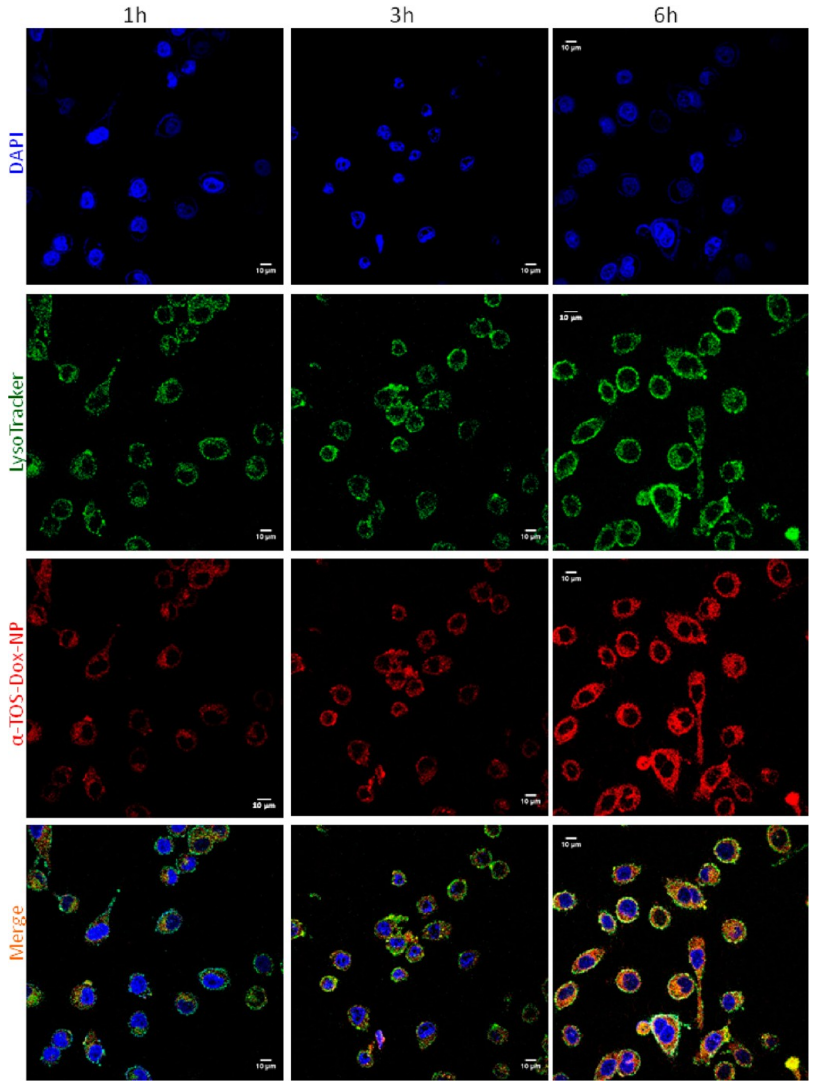

Figure 4. Cellular internalization of α-TOS-Dox-NP in HeLa cells in 1, 3, and 6 h time points observed by confocal laser scanning microscopy (CLSM). Lysosomal compartments and nuclei were stained with LysoTracker Green DND-26 (green) and DAPI (blue), respectively. Merged images (yellow) show the internalization of α-TOS-Dox-NP in lysosomal compartments. Scale bar = 10 μm.

NP, α-TOS-Dox-NP, and α-TOS-Paclitaxel-NP, respectively. This caspase assay clearly demonstrated that different dual drug conjugated nanoparticles induced apoptosis in HeLa cells.

3.2.4. Cell Cycle Analysis. To understand the mechanism of action further, we evaluated the effect of different dual drug conjugated nanoparticles on cell cycle. We analyzed the cell cycle arrest by using propidium iodide (PI)-labeled DNA in HeLa cells after 24h post-treatment. The flow cytometry analysis showed that after α-TOS-CDDP-NP treatment, cells were in G1, S and G2-M phase as 67.9%, 32.1%, and 0% respectively, whereas, non treated cells were found to be as 38.1%, 49.2%, and 12.5%, respectively (Figure 3e). Similarly, after α-TOS-Dox-NP treatment, 30.7%, 51.0%, and 18.3% cells were found to be in G1, S, and G2-M phase, respectively. Finally, α-TOS-Paclitaxel-NP treated cells were found as 26.2%, 52.9%, and 23.4% in G1, S and G2-M phase, respectively. From this cell cycle analysis, it was evident that α-TOS-CDDP-NP arrested the cells in G1 phase whereas α-TOS-Dox-NP and α-TOS-Paclitaxel-NP arrested the HeLa cells in G2-M phase.

3.3. Cellular Internalization of Dual Drug Conjugated Nanoparticles. To visualize the temporal cellular internalization mechanism of the dual drug conjugated nanoparticles, we treated the HeLa cells with red fluorescent α-TOS-Dox-NP (2 μg/mL of doxorubicin concentration) for 1 h, 3 h and 6 h time points. We treated the cells with 2 μg/mL of free doxorubicin as control. We stained the low pH lysosomal compartments with LysoTracker Green DND-26 (green) and nucleus with 4′,6-diamidino-2-phenylindole (DAPI)(blue) respectively and imaged the cells by using high resolution confocal laser scanning microscopy (CLSM) (Figure 4 and Figure S27 in Supporting Information). From Figure 4, it was clear that α-TOS-Dox-NPs were internalized into the cells in a time dependent manner over 6 h and homed into the lysosomal compartments, which led the colocalization of red and green fluorescence resulting yellow color. We also quantified the amount of colocalization of green and red fluorescence through Pearsons' correlation coefficient and Manders coefficients by CLSM. It was found that the percent volume of colocalization increased from 1 to 3 to 6 h by 18.6% to 21.5% to 40.7% (Table S1 in Supporting Information). In contrast, free doxorubicin internalized into the cells within 3 h and directly localized into the nucleus, which led the colocalization of red and blue fluorescence resulting purple color (Figure S27 in Supporting Information). Interestingly, in free doxorubicin treatment, no

DOI: 10.1021/am5090226
ACS Appl. Mater. Interfaces 2015, 7, 7584−7598

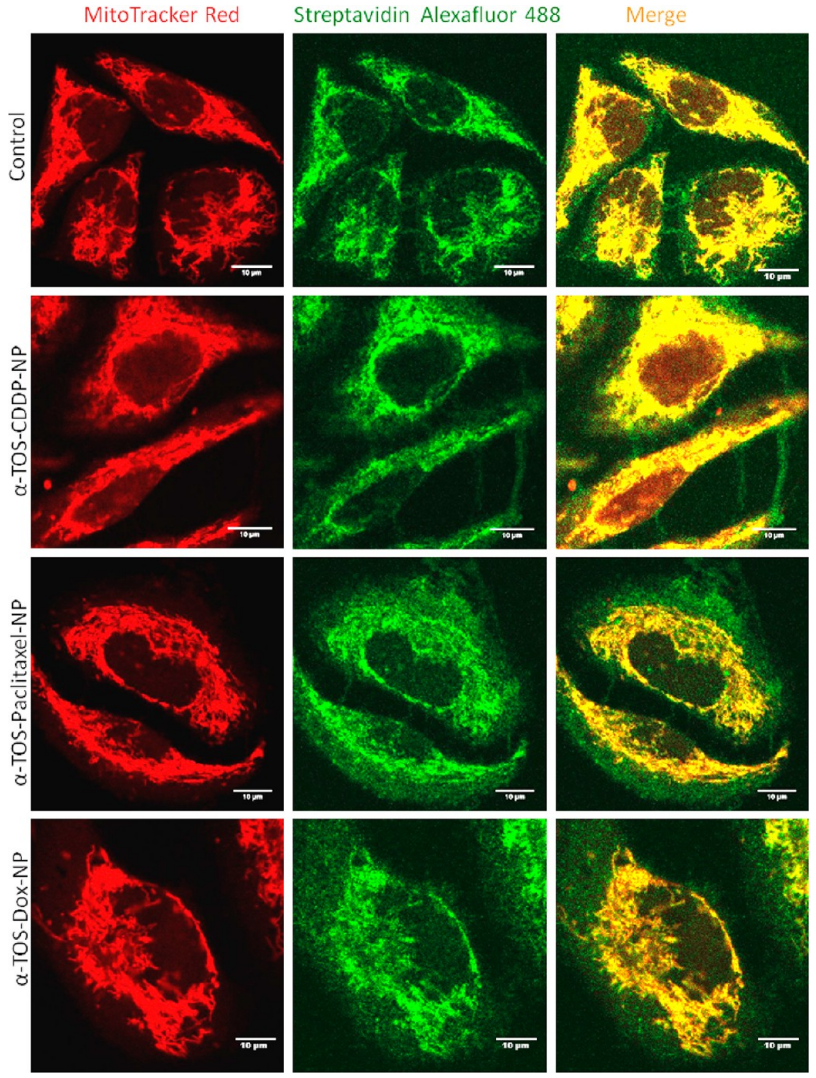

Figure 5. CLSM of mitochondria after treatment with individual dual drug conjugated nanoparticles for 24 h. Mitochondria were stained with MitoTracker Red CMXROS (red) and biotinylated proteins overexpressed on mitochondria were stained with Streptavidine Alexaflour 488 (green). CLSM images show the damage of mitochondrial morphology with different dual drug conjugated nanoparticle treatments. Scale bar = 10 μm.

colocalization of green and red was observed which clearly demonstrated that free doxorubicin was internalized into the cell through diffusion pathway and homed directly into nucleus. To further visualize the internalization of α-TOS-CDDP-NP and α-TOS-Paclitaxel-NP, we encapsulated a red fluorescent dye rhodamine to synthesize α-TOS-CDDP-Rho-NP and α-TOS-Paclitaxel-Rho-NP respectively. We incubated the HeLa cells with α-TOS-CDDP-Rho-NP and α-TOS-Paclitaxel-Rho-NP for 1 h, 3 h and 6 h time points. We stained the lysosomal compartment and nucleus with LysoSensor Green DND-153 (green) and DAPI (blue) respectively. The CLSM images and colocalization quantification (Figure S28 and Table S2 in Supporting Information) clearly showed that α-TOS-CDDP-Rho-NP internalized into the lysosomal compartment within 1 h (26.2% colocalization) and retained for 6 h (31.1% colocalization). Similarly, α-TOS-Paclitaxel-Rho-NP also internalized into lysosomal compartments within 1 h (30.2% colocalization) and retained there for 6 h (29.2% colocalization)(Figure S29 and Table S3 in Supporting Information). The CLSM images and colocalization quantification data clearly showed that dual drug conjugated nanoparticles were internalized into the HeLa cells through endocytosis into the acidic lysosomal compartments in a temporal manner in contrast to the free drugs.

3.4. Targeting Mitochondria by Dual Drug Conjugated Nanoparticles. We hypothesized that after internalization of dual drug conjugated nanoparticles into lysosomal compartments, the individual drugs will be released to target mitochondria and nucleus. Hence, we evaluated the effect of dual drug conjugated nanoparticles on mitochondrial morphology. We treated HeLa cells with different dual drug conjugated nanoparticles individually for 24 h at their respective IC_{50} drug dosages and stained the mitochondia with red fluorescent MitoTracker Red CMXROS (Figure 5). We also costained the endogenous biotinylated proteins prevalent in mitochondria[62] by green fluorescent Streptavidin Alexaflour 488 and visualized the mitochondrial morphology change by CLSM. From Figure 5, it was clear that the nontreated control cells showed nice elongated mitochondrial morphology, which was visibly disrupted, leading to the mitochondrial fragmentation in different nanoparticle treated cells. Colocalization of MitoTracker Red CMXROS (red) and Streptavidine Alexaflour 488 (green) leading to yellow color in the merged images clearly demonstrated the lack of characteristic mitochondrial morphol-

DOI: 10.1021/am5090226
ACS Appl. Mater. Interfaces 2015, 7, 7584−7598

ogy by different nanoparticle treatments. Moreover, we quantified the average mitochondrial area by using ImageJ analysis software with the help of Mito-Morphology macro, which allows to measure mitochondrial elongation, interconnectivity and morphology from epifluorescence images of cells stained for mitochondria.[63] The mitochondrial average area for a non treated cell was found to be 10.1 ± 0.6 μm^2, whereas the average fragmented mitochondria area was found to be reduced to 5.7 ± 1.0, 3.1 ± 0.6, and 4.9 ± 0.9 μm^2 for α-TOS-CDDP-NP, α-TOS-Dox-NP, and α-TOS-Paclitaxel-NP treated cells, respectively (n = 5, mean ± SEM) (Figure S30 in Supporting Information). From these CLSM images and quantification of the average mitchondrial area, it is clear that α-TOS from different dual drug conjugated nanoparticles targeted mitochondria and exhibited mitochondrial fragmentation. One of the hallmarks of mitochondrial damage is the mitochondrial outer membrane permeabilization (MOMP) followed by release of cytochrome c from intermembrane spaces (IMS).[64] We treated HeLa cells with different dual drug conjugated nanoparticles at their respective IC_{50} drug dosages for 24 h. The cells were then fixed and stained with green fluorescent Alexafluor 488 antibody specific for cytochrome c and visualized by CLSM. From Figure 6a, it is clear that α-TOS-CDDP-NP, α-TOS-Dox-NP, and α-TOS-Paclitaxel-NP showed highly increased amount of cytochrome c expression in HeLa cells compared to non treated control cells. We also determined the expression of cytochrome c by Western blot analysis using cytochrome c rabbit monoclonal antibody, after treatment of HeLa cells with different dual drug conjugated nanoparticles at their respective IC_{50} drug dosages for 24 h. From the Western blot images (Figure 6b), it was clear that all three dual drug conjugated nanoparticles increased the expression level of cytochrome c compared to the non treated control. Moreover, we also quantified the expression level of cytochrome c from the Western blot, which clearly showed 1.1-fold, 1.5-fold and 1.5-fold increased expression of cytochrome c after the treatment with α-TOS-CDDP-NP, α-TOS-Dox-NP and α-TOS-Paclitaxel-NP respectively compared to the non treated control (Figure S31 in Supporting Information). From these CLSM images of mitochondrial morphology, cytochrome c release by inducing MOMP, Western blot analysis and quantification, it was clear that the dual drug conjugated nanoparticles damaged mitchondria in the HeLa cancer cells.

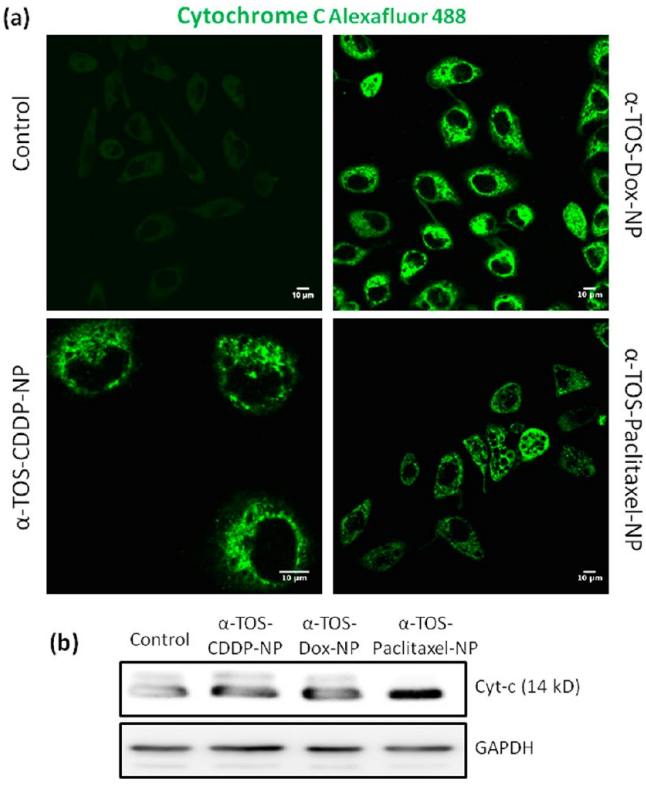

Figure 6. Characterization of mitochondrial damage by cytochrome c expression. (a) CLSM images of dual drug conjugated nanoparticle treated HeLa cells for 24h at their respective IC_{50} drug dosages compared to nontreated control. Cells were stained with cytochrome c-Alexafluor 488 antibody (green). Scale bar = 10 μm. (b) The expression of cytochrome c in HeLa cells after 24 h post incubation with dual drug conjugated nanoparticles determined by Western blot analysis.

3.5. Targeting Nucleus and Microtubule by Dual Drug Conjugated Nanoparticle. Nucleus contains the genomic materials (DNA and RNA), regulates the gene expression and controls the replication of DNA during cell cycle. Hence damaging the DNA in the nucleus of the cancer cells would lead to inhibit the rapid cellular division. The DNA damage in the nucleus is followed by the phosphorylation of the histone H2AX in recruiting and localizing the DNA damage repairing proteins. Hence, γH2AX has evolved as one of the important biomarkers to observe DNA damage.[65] To determine the effect of dual drug conjugated nanoparticles in nucleus we treated the HeLa cells with different dual drug conjugated nanoparticles in their respective IC_{50} drug dosages for 24 h. We stained the cells with green fluorescent Alexafluor 488 antibody specific for γH2AX and visualized the expression of γH2AX by CLSM. From Figure 7a, it was clear that α-TOS-CDDP-NP inflicted high DNA damage in nucleus to induce elevated expression of γH2AX compared to nontreated control. α-TOS-Dox-NP induced lower level of γH2AX expression compared to α-TOS-CDDP-NP treatment. It was reported that doxorubicin promoted histone eviction leading to induce lower expression of γH2AX.[66] Finally, we observed minimum expression γH2AX after α-TOS-Paclitaxel-NP, which was expected as paclitaxel does not induce DNA damage directly.

We also evaluated the expression of γH2AX by Western blot analysis after 24 h incubation of HeLa cells with different dual drug conjugated nanoparticles in their respective IC_{50} drug dosages. From the Western blot image (Figure 7b), it was clear that α-TOS-CDDP-NP induced highest level of γH2AX expression compared to α-TOS-Dox-NP, α-TOS-Paclitaxel-NP, as well as nontreated control. We also quantified the relative expression of γH2AX in different dual drug conjugated nanoparticle treatments from Western blot analysis. We observed 9.1 fold, 6.5 fold and 1.4 fold increases in γH2AX expression induced by α-TOS-CDDP-NP, α-TOS-Dox-NP, and α-TOS-Paclitaxel-NP, respectively, compared to the nontreated control (Figure S32 in Supporting Information).

Nuclear DNA damage triggers poly(ADP-ribose) polymerase (PARP) family of proteins, which are involved in a number of cellular processes mainly DNA repair and apoptosis. Hence, PARP activation has emerged as one of the biomarkers for cellular DNA damage.[67] We treated the HeLa cells with different dual drug conjugated nanoparticles in their respective IC_{50} drug dosages for 24 h followed by staining with greeen fluorescent Alexafluor 488 antibody specific to PARP. We visualized the PARP expression by using CLSM. From Figure

DOI: 10.1021/am5090226
ACS Appl. Mater. Interfaces 2015, 7, 7584−7598

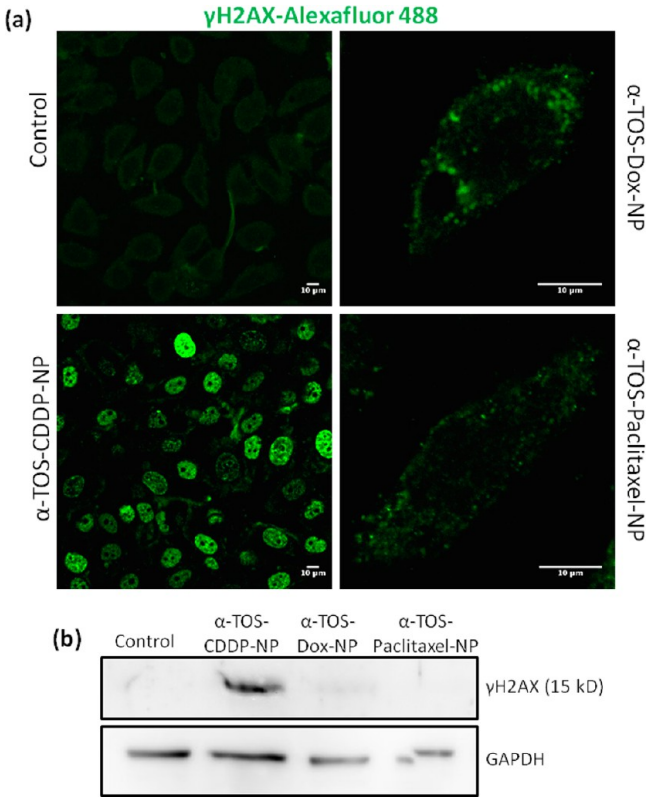

Figure 7. Characterization of nuclear damage by γH2AX as DNA damage marker. (a) CLSM images of dual drug conjugated nanoparticle treatments to HeLa cells for 24 h at their respective IC_{50} drug dosages compared to nontreated control. Cells were stained with γH2AX-Alexafluor 488 antibody (green). Scale bar = 10 μm. (b) The expression of γH2AX in HeLa cells after 24h post incubation with dual drug conjugated nanoparticles determined by Western blot analysis.

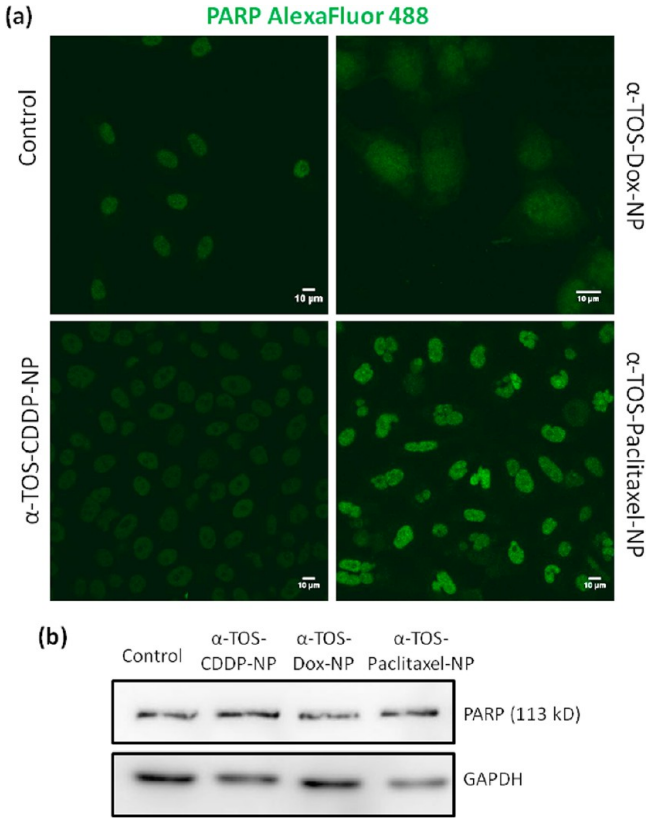

Figure 8. Characterization of nuclear damage by PARP as DNA damage repair marker. (a) CLSM images of dual drug conjugated nanoparticle treatments to HeLa cells for 24 h at their respective IC_{50} drug dosages compared to nontreated control. Cells were stained with PARP-Alexafluor 488 antibody (green). Scale bar = 10 μm. (b) The expression of PARP (113 kDa) in HeLa cells after 24 h post incubation with dual drug conjugated nanoparticles determined by Western blot analysis.

8a, it was clear that interestingly α-TOS-Paclitaxel-NP induced highest PARP expression compared to α-TOS-CDDP-NP and α-TOS-Dox-NP. However, all the dual drug conjugated nanoparticles induced increased amount of PARP compared to nontreated cells. We further treated the HeLa cells with different dual drug conjugated nanoparticles and evaluated the expression of PARP by using Western blot analysis. The Western blot image (Figure 8b) showed improved PARP expression after treatment with different nanoparticles compared to control cells. Moreover, the normalized PARP quantification from Western blot clearly demonstrated that α-TOS-CDDP-NP, α-TOS-Dox-NP and α-TOS-Paclitaxel-NP induced 3.1-fold, 1.3-fold, and 4.8-fold, respectively (Figure S33 in Supporting Information).

Furthermore, we also observed the effect of different dual drug conjugated nanoparticles on morphology of the nucleus. We treated HeLa cells with dual drug conjugated nanoparticles with respective IC_{50} drug dosages for 24 h and stained the nucleus with blue fluorescent 4′,6-diamidino-2-phenylindole (DAPI). We visualized the morphology of nucleus by CLMS. Only α-TOS-Paclitaxel-NP induced the fragmentation of nucleus (Figure 9, indicated by bold arrows). On the other hand, α-TOS-CDDP-NP and α-TOS-Dox-NP showed almost negligible clustering of nucleus compared to the control (Figure 9). It was reported that paclitaxel and other microtubule binding drugs induce the clustering of nucleus.[68] Hence, it was clear that free paclitaxel released from α-TOS-Paclitaxel-NP was responsible for observed nuclear clustering. We also costained tubulin with green fluorescent tubulin Alexafluor 488 anitbody and visualized the effect of dual drug conjugated nanoparticles. From Figure 9 it was clear that only α-TOS-Paclitaxel-NP disrupted the typical elongated morphology of tubulin (indicated by thin arrows in Figure 9) into small fragments, whereas α-TOS-CDDP-NP and α-TOS-Dox-NP showed almost no tubulin damage compared to control. We anticipated this effect of α-TOS-Paclitaxel-NP compared to α-TOS-CDDP-NP and α-TOS-Dox-NP, as paclitaxel is known to bind with mircotubule. From these CLSM, Western blot analysis and protein expression quantification it was clear that all the dual drug conjugated nanoparticles damaged nuclear DNA as well as tubulin in HeLa cancer cells.

4. CONCLUSION

We have successfully developed dual drug conjugates by direct attachment of mitochondria damaging drug (α-TOS) and clinically approved DNA damaging drugs (cisplatin and doxorubicin) or microtubule binding drug (paclitaxel) without any additional linker strategy. We engineered sub 200 nm particles from those dual drug conjugates and characterized them by different electron microscopy (FESEM, TEM, and AFM) techniques. These nanoparticles released the dual drugs in a slow and sustained manner over 3 days at pH = 5.5 mimicking the lysosomal compartments inside the tumor cells.

DOI: 10.1021/am5090226
ACS Appl. Mater. Interfaces 2015, 7, 7584−7598

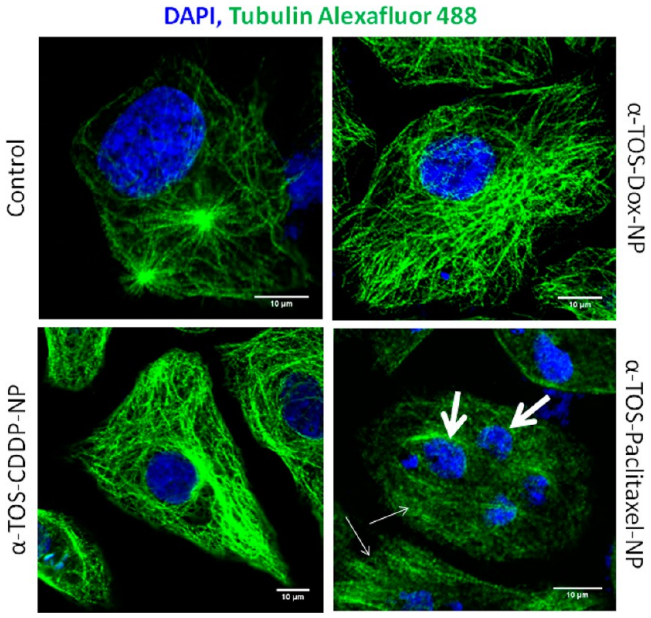

Figure 9. Characterization of nuclear fragmentation and tubulin damage after treatment with dual drug conjugated nanoparticles at 24 h postincubation in HeLa cells. Nucleus was stained with DAPI (blue), and tubulin was stained with tubulin-Alexafluor 488 antibody. Nuclear fragmentation is indicated by bold arrows and tubulin damage is indicated by thin arrows. Scale bar = 10 μm.

Indeed these nanoparticles internalized into the lysosomal compartments in a time depedent manner through endocytosis in HeLa cervical cancer cells visualized by CLSM. These nanoparticles showed cytotoxicity by inducing apoptosis through arresting cell cycle. These nanoparticles damaged the mitochondrial morphology and released cytochome c. These dual drug conjugated nanoparticles damaged the nucleus of HeLa cells and expressed DNA damaging marker γH2AX, DNA repair marker PARP. α-TOS-Paclitaxel-NP also damaged the tubulin of the HeLa cells. We anticipate that these dual drug conjugated nanoparticle strategy can be used as platform technology to conjugate different organelle damaging drugs and target them to illuminate the organelle cross talk in a diseased state like cancer. Moroever, these dual drug conjugated nanoparticles can be easily translated to the clinics to develop novel next generation multiple organelle damaging combination cancer therapeutics which can lead to reduced toxic side effects from the individual drugs, thus overcome drug resistance and providing a better quality of life to the cancer patients.

■ ASSOCIATED CONTENT

Ⓢ Supporting Information

Chemical characterization by NMR, mass spectroscopy, UV−vis spectroscopy, DLS, AFM, EDX and biological evaluation details. This material is available free of charge via the Internet at http://pubs.acs.org.

■ AUTHOR INFORMATION

Corresponding Author

*E-mail: sudipta.basu@iiserpune.ac.in.

Present Address

B.A.C.: Vice-Chancellor, Dr. Babasaheb Ambedkar Marathwada University, Aurangabad, 431004, India.

Author Contributions

A.M. and P.M. contributed equally to this work.

Notes

The authors declare no competing financial interest.

■ ACKNOWLEDGMENTS

We sincerely thank the Director, IISER-Pune, DBT (Ramalingaswami Fellowship) and SERB (Fast Track Scheme for Young Scientist) for financial support. We thank Dr. Shouvik Datta for FE-SEM images. We thank Department of Science and Technology (DST) Nanoscience unit for providing AFM facility. We thank Nimisha Parekh and Polymer Science and Engineering Division at CSIR-NCL to provide FACS facility. We also thank Nitheesh K, Dnyanesh Dubal, Vijay Vittal and Dr. Richa Rikhy from IISER Pune for helping in capturing CLSM images. Finally, AM thanks CSIR-UGC for providing the doctoral fellowship.

■ REFERENCES

(1) Ferlay, J.; Shin, H.-R.; Bray, F.; Forman, D.; Mathers, C.; Parkin, D. M. Estimates of Worldwide Burden of Cancer in 2008: GLOBOCAN 2008. *J. Cancer* **2010**, *127*, 2893−2917.

(2) Siegel, R.; Ma, J.; Zou, Z.; Jemal, A. Cancer Statistics, 2014. *CA Cancer J. Clin.* **2014**, *64*, 9−29.

(3) DeVita, V. T., Jr.; Chu, E. A History of Cancer Chemotherapy. *Cancer Res.* **2008**, *68*, 8643−8653.

(4) Knight, Z. A.; Lin, H.; Shokat, K. M. Targeting the Cancer Kinome Through Polypharmacology. *Nat. Rev. Cancer* **2010**, *10*, 130−137.

(5) Holohan, C.; Schaeybroeck, S. V.; Longley, D. B.; Johnston, P. G. Cancer Drug Resistance: an Evolving Paradigm. *Nat. Rev. Cancer* **2013**, *13*, 714−726.

(6) Jia, J.; Zhu, F.; Ma, X.; Cao, Z. W.; Li, Y. X.; Chen, Y. Z. Mechanisms of Drug Combinations: Interaction and Network Perspectives. *Nat. Rev. Drug Discovery* **2009**, *8*, 111−128.

(7) Al-Lazikani, B.; Banerji, U.; Workman, P. Combinatorial Drug Therapy for Cancer in the Post-Genomic Era. *Nat. Biotechnol.* **2012**, *30*, 679−692.

(8) Nummari, J.; Suomalainen, A. Mitochondria: In Sickness and in Health. *Cell* **2012**, *148*, 1145−1159.

(9) Galluzzi, L.; Kepp, O.; Kroemer, G. Mitochondria: Master Regulators of Danger Signalling. *Nat. Rev. Mol. Cell Biol.* **2012**, *13*, 780−788.

(10) Chamberlain, G. R.; Tulumello, D. V.; Kelley, S. O. Targeted Delivery of Doxorubicin to Mitochondria. *ACS Chem. Biol.* **2013**, *8*, 1389−1395.

(11) Wisnovsky, S. P.; Wilson, J. J.; Radford, R. J.; Pereira, M. P.; Chan, M. R.; Laposa, R. R.; Lippard, S. J.; Kelley, S. O. Targeting Mitochondrial DNA with a Platinum-Based Anticancer Agent. *Chem. Biol.* **2013**, *20*, 1323−1328.

(12) Marrache, S.; Pathaka, R. K.; Dhar, S. Detouring of Cisplatin to Access Mitochondrial Genome for Overcoming Resistance. *Proc. Natl. Acad. Sci. U.S.A.* **2014**, *111*, 10444−10449.

(13) Pathak, R. K.; Marrache, S.; Harn, D. A.; Dhar, S. Mito-DCA: A Mitochondria Targeted Molecular Scaffold for Efficacious Delivery of Metabolic Modulator Dichloroacetate. *ACS Chem. Biol.* **2014**, *9*, 1178−1187.

(14) Dhar, S.; Lippard, S. J. Mitaplatin, A Potent Fusion of Cisplatin and the Orphan Drug Dichloroacetate. *Proc. Natl. Acad. Sci. U.S.A.* **2009**, *106*, 22199−22204.

(15) Suntharalingam, K.; Song, Y.; Lippard, S. J. Conjugation of Vitamin E Analog α-TOS to Pt(IV) Complexes for Dual-Targeting Anticancer Therapy. *Chem. Commun.* **2014**, *50*, 2465−2468.

(16) Ward, P. S.; Thompson, C. B. Metabolic Reprogramming: a Cancer Hallmark Even Warburg Did Not Anticipate. *Cancer Cell* **2012**, *21*, 297−308.

DOI: 10.1021/am5090226
ACS Appl. Mater. Interfaces 2015, 7, 7584−7598

(17) Guo, J. Y.; Xia, B.; White, E. Autophagy-Mediated Tumor Promotion. *Cell* **2013**, *155*, 1216−1219.
(18) Peer, D.; Karp, J. M.; Hong, S.; Farokhzad, O. C.; Margalit, R.; Langer, R. Nanocarriers as an Emerging Platform for Cancer Therapy. *Nat. Nanotechnol.* **2007**, *2*, 751−760.
(19) Castanotto, D.; Rossi, J. J. The Promises and Pitfalls of RNA-Interference-Based Therapeutics. *Nature* **2009**, *457*, 426−433.
(20) Matsumura, Y.; Maeda, H. A New Concept for Macromolecular Therapeutics in Cancer Chemotherapy: Mechanism of Tumoritropic Accumulation of Proteins and the Antitumor Agent Smancs. *Cancer Res.* **1986**, *46*, 6387−6392.
(21) Ruoslahti, E.; Bhatia, S. N.; Sailor, M. J. Targeting of Drugs and Nanoparticles to Tumors. *J. Cell Biol.* **2010**, *188*, 759−68.
(22) Couvreur, P.; Vauthier, C. Nanotechnology: Intelligent Design to Treat Complex Disease. *Pharm. Res.* **2001**, *74*, 1417−1450.
(23) Kolishettia, N.; Dhar, S.; Valencia, P. M.; Lin, L. Q.; Karnik, R.; Lippard, S. J.; Langer, R.; Farokhzad, O. C. Engineering of Self-Assembled Nanoparticle Platform for Precisely Controlled Combination Drug Therapy. *Proc. Natl. Acad. Sci. U.S.A.* **2010**, *107*, 17939−17944.
(24) Wang, H.; Zhao, Y.; Wu, Y.; Hu, Y.; Nan, K.; Nie, N.; Chen, H. Enhanced Anti-Tumor Efficacy by Co-Delivery of Doxorubicin and Paclitaxel with Amphiphilic Methoxy PEG-PLGA Copolymer Nanoparticles. *Biomaterials* **2011**, *32*, 8281−8290.
(25) Liao, L.; Liu, J.; Dreaden, E. C.; Morton, S. W.; Shopsowitz, K. E.; Hammond, P. T.; Johnson, J. A. A Convergent Synthetic Platform for Single-Nanoparticle Combination Cancer Therapy: Ratiometric Loading and Controlled Release of Cisplatin, Doxorubicin, and Camptothecin. *J. Am. Chem. Soc.* **2014**, *136*, 5896−5899.
(26) Sengupta, S.; Eavarone, D.; Capila, I.; Zhao, G.; Watson, N.; Kiziltepe, T.; Sasisekharan, R. Temporal Targeting of Tumour Cells and Neovasculature with a Nanoscale Delivery System. *Nature* **2005**, *436*, 568−572.
(27) Deng, Z. J.; Morton, S. W.; Ben-Akiva, E.; Dreaden, E. C.; Shopsowitz, K. E.; Hammond, P. T. Layer-By-Layer Nanoparticles for Systemic Codelivery of an Anticancer Drug and siRNA for Potential Triple-Negative Breast Cancer Treatment. *ACS Nano* **2013**, *7*, 9571−9584.
(28) Zhang, L.; Xia, J.; Zhao, Q.; Liu, L.; Zhang, Z. Functional Graphene Oxide as a Nanocarrier for Controlled Loading and Targeted Delivery of Mixed Anticancer Drugs. *Small* **2010**, *6*, 537−544.
(29) Jiang, T.; Mo, R.; Bellotti, A.; Zhou, J.; Gu, Z. Gel−Liposome-Mediated Co-Delivery of Anticancer Membrane-Associated Proteins and Small-Molecule Drugs for Enhanced Therapeutic Efficacy. *Adv. Funct. Mater.* **2014**, *24*, 2295−2304.
(30) Chin, C. F.; Yap, S. Q.; Li, J.; Pastorin, G.; Ang, W. H. Ratiometric Delivery of Cisplatin and Doxorubicin Using Tumour-Targeting Carbon-Nanotubes Entrapping Platinum(IV) Prodrugs. *Chem. Sci.* **2014**, *5*, 2265−2270.
(31) Marrache, S.; Dhar, S. Engineering of Blended Nanoparticle Platform for Delivery of Mitochondria-Acting Therapeutics. *Proc. Natl. Acad. Sci. U.S.A.* **2012**, *109*, 16288−16293.
(32) Marrache, S.; Dhar, S. The Energy Blocker Inside the Power House: Mitochondria Targeted Delivery of 3-Bromopyruvate. *Chem. Sci.* **2014**, *6*, 1832−1845.
(33) Singh, K. K.; Kulawiec, M.; Still, I.; Desouki, M. M.; Geradts, J.; Matsui, S. Inter-Genomic Cross Talk Between Mitochondria and the Nucleus Plays an Important Role in Tumorigenesis. *Gene* **2005**, *354*, 140−146.
(34) Rowland, A. A.; Voeltz, G. K. Endoplasmic Reticulum−Mitochondria Contacts: Function of the Junction. *Nat. Rev. Mol. Cell Biol.* **2012**, *13*, 607−615.
(35) Bernhard, W.; Granboulan, N. The Fine Structure of the Cancer Cell Nucleus. *Exp. Cell Res.* **1963**, *24*, 19−53.
(36) Neuzil, J.; Webe, T.; Shroder, A.; Lu, M.; Ostermann, G.; Gellert, N.; Mayne, G. C.; Olejnicka, B.; Negre-Salvayre, A.; Sticha, M.; Coffe, R. J.; Weber, C. Induction of Cancer Cell Apoptosis by Alpha-Tocopheryl Succinate: Molecular Pathways and Structural Requirements. *FASEB J.* **2001**, *15*, 403−415.
(37) Prasad, K. N.; Edwords-Prasad, J. Activation of Extracellular Signal-Regulated Kinase and c-Jun-NH(2)-Terminal Kinase but not p38 Mitogen-Activated Protein Kinases is Required for RRR-Alpha-Tocopheryl Succinate-Induced Apoptosis of Human Breast Cancer Cells. *Cancer Res.* **2001**, *61*, 6569−6576.
(38) Zhang, Y.; Ni, J.; Messing, E. M.; Chang, E.; Yang, C. R.; Yeh, S. Vitamin E Succinate Inhibits the Function of Androgen Receptor and the Expression of Prostate-Specific Antigen in Prostate Cancer Cells. *Proc. Natl. Acad. Sci. U.S.A.* **2002**, *99*, 7408−7413.
(39) Prochazka, L.; Dong, L.; Valis, K.; Freeman, R.; Ralph, S. J.; Turanek, J.; Neuzil, J. Alpha-Tocopheryl Succinate Causes Mitochondrial Permeabilization by Preferential Formation of Bak Channels. *Apoptosis* **2010**, *15*, 782−794.
(40) Dong, L. F.; Low, P.; Dyason, J. C.; Wang, X. F.; Prochazka, L.; Witting, P. K.; Freeman, R.; Swettenham, E.; Valis, K.; Liu, J.; Zobalova, R.; Turanek, J.; Spitz, D. R.; Domann, F. E.; Scheffler, I. E.; Ralph, S. J.; Neuzil, J. Alpha-Tocopheryl Succinate Induces Apoptosis by Targeting Ubiquinone-Binding Sites in Mitochondrial Respiratory Complex II. *Oncogene* **2008**, *27*, 4324−4335.
(41) Dong, L.; Freeman, R.; Liu, J.; Zobalova, R.; Marin-Hernandez, A.; Stantic, M.; Rohlena, J.; Valis, K.; Rodriguez-Enriquez, S.; Butcher, B.; Goodwin, J.; Brunk, U. T.; Witting, P. K.; Moreno-Sanchez, R.; Scheffler, I. E.; Ralph, S. J.; Neuzil, J. Suppression of Tumor Growth In Vivo by the Mitocan Alpha-Tocopheryl Succinate Requires Respiratory Complex II. *Clin. Cancer Res.* **2009**, *15*, 1593−1600.
(42) Kruspig, B.; Zhivotovsky, B.; Gogvadze, V. Contrasting Effects of α-Tocopheryl Succinate on Cisplatin- and Etoposide-Induced Apoptosis. *Mitochondrion* **2013**, *13*, 533−538.
(43) Zhang, X.; Peng, X.; Yu, W.; Hou, S.; Zhao, Y.; Zhang, Z.; Huang, X.; Wua, K. Alpha-Tocopheryl Succinate Enhances Doxorubicin-Induced Apoptosis in Human Gastric Cancer Cells Via Promotion of Doxorubicin Influx and Suppression of Doxorubicin Efflux. *Cancer Lett.* **2011**, *307*, 174−181.
(44) Kanai, K.; Kikuchi, E.; Mikami, S.; Suzuki, E.; Uchida, Y.; Kodaira, K.; Miyajima, A.; Ohigashi, T.; Nakashima, J.; Oya, M. Vitamin E Succinate Induced Apoptosis and Enhanced Chemosensitivity to Paclitaxel in Human Bladder Cancer Cells In Vitro and In Vivo. *Cancer Sci.* **2010**, *101*, 216−223.
(45) Neuzil, J.; Weber, T.; Gellert, N.; Weber, C. Selective Cancer Cell Killing by Alpha-Tocopheryl Succinate. *Br. J. Cancer.* **2001**, *84*, 87−89.
(46) Crispen, P. L.; Uzzo, R. G.; Golovine, K.; Makhov, P.; Pollack, A.; Horwitz, E. M.; Greenberg, R. E.; Kolenko, V. M. Vitamin E Succinate Inhibits NF-KappaB and Prevents the Development of a Metastatic Phenotype in Prostate Cancer Cells: Implications for Chemoprevention. *Prostate* **2007**, *67*, 582−590.
(47) Yao, X.; Panichpisal, K.; Kurtzman, N.; Nugent, K. Cisplatin Nephrotoxicity: A Review. *Am. J. Med. Sci.* **2007**, *334*, 115−124.
(48) Octavia, Y.; Tocchetti, C. G.; Gabrielson, K. L.; Janssens, S.; Crijns, H. J.; Moens, A. L. Doxorubicin-Induced Cardiomyopathy: from Molecular Mechanisms to Therapeutic Strategies. *J. Mol. Cell. Cardiol.* **2012**, *52*, 1213−25.
(49) Rowinsky, E. K.; Chaudhry, V.; Cornblath, D. R.; Donehower, R. C. Neurotoxicity of Taxol. *J. Natl. Cancer Inst. Monogr.* **1993**, *15*, 107−115.
(50) Aronov, O.; Horowitz, A. T.; Gabizon, A.; Gibson, D. Folate-Targeted PEG as a Potential Carrier for Carboplatin Analogs. Synthesis and In Vitro Studies. *Bioconjugate Chem.* **2003**, *14*, 563−574.
(51) Brown, S. D.; Nativo, P.; Smith, J.-A.; Stirling, D.; Edwards, P. R.; Venugopal, B.; Flint, D. J.; Plumb, J. A.; Graham, D.; Wheate, N. J. Gold Nanoparticles for the Improved Anticancer Drug Delivery of the Active Component of Oxaliplatin. *J. Am. Chem. Soc.* **2010**, *132*, 4678−4684.
(52) Still, B. M.; Kumar, P. G.; Aldrich-Wright, J. R.; Price, W. S. ^{195}Pt NMR-Theory and Application. *Chem. Soc. Rev.* **2007**, *36*, 665−686.

DOI: 10.1021/am5090226
ACS Appl. Mater. Interfaces 2015, 7, 7584−7598

(53) Sengupta, P.; Basu, S.; Soni, S.; Pandey, A.; Roy, B.; Oh, M. S.; Chin, K. T.; Paraskar, A. S.; Sarangi, S.; Connor, Y.; Sabbisetti, V. S.; Kopparam, J.; Kulkarni, A.; Muto, K.; Amarasiriwardena, C.; Jayawardene, I.; Lupoli, N.; Dinulescu, D.; Bonventre, J. V.; Mashelkar, R. A.; Sengupta, S. Cholesterol-Tethered Platinum II-Based Supramolecular Nanoparticle Increases Antitumor Efficacy and Reduces Nephrotoxicity. *Proc. Natl. Acad. Sci. U.S.A.* **2012**, *109*, 11294−11299.
(54) Li, K.; Liu, B. Polymer-Encapsulated Organic Nanoparticles for Fluorescence and Photoacoustic Imaging. *Chem. Soc. Rev.* **2014**, *43*, 6570−6597.
(55) Harris, J. M.; Chess, R. B. Effect of Pegylation on Pharmaceuticals. *Nat. Rev. Drug Discovery* **2003**, *2*, 214−221.
(56) Gilleron, J.; Querbes, W.; Zeigerer, A.; Borodovsky, A.; Marsico, G.; Schubert, U.; Manygoats, K.; Seifert, S.; Andree, C.; Stöter, M.; Epstein-Barash, H.; Zhang, L.; Koteliansky, V.; Fitzgerald, K.; Fava, E.; Bickle, M.; Kalaidzidis, Y.; Akinc, A.; Maier, M.; Zerial, M. Image-Based Analysis of Lipid Nanoparticle-Mediated siRNA Delivery, Intracellular Trafficking and Endosomal Escape. *Nat. Biotechnol.* **2013**, *31*, 638−646.
(57) Prochazka, L.; Koudelka, S.; Dong, L.-F.; Stursa, J.; Goodwin, J.; Neca, J.; Slavik, J.; Ciganek, M.; Masek, J.; Kluckova, K.; Nguyen, M.; Turanek, J.; Neuzil, J. Mitochondrial Targeting Overcomes ABCA1-Dependent Resistance of Lung Carcinoma to α-Tocopheryl Succinate. *Apoptosis* **2013**, *18*, 286−299.
(58) Chou, T.-C. Drug Combination Studies and Their Synergy Quantification Using the Chou-Talalay Method. *Cancer Res.* **2010**, *70*, 440−446.
(59) Mariño, G.; Niso-Santano, M.; Baehrecke, E. H.; Kroemer, G. Self-Consumption: The Interplay of Autophagy and Apoptosis. *Nat. Rev. Mol. Cell Biol.* **2014**, *15*, 81−94.
(60) Kruidering, M.; Evan, G. I. Caspase-8 in Apoptosis: The Beginning of "the End"? *IUBMB Life* **2000**, *50*, 85−90.
(61) Li, P.; Nijhawan, D.; Budihardjo, I.; Srinivasula, S. M.; Ahmad, M.; Alnemri, E. S.; Wang, X. Cytochrome c and dATP-Dependent Formation of Apaf-1/Caspase-9 Complex Initiates an Apoptotic Protease Cascade. *Cell* **1997**, *91*, 479−489.
(62) Chapman-Smith, A.; Cronan, J. E., Jr. In Vivo Enzymatic Protein Biotinylation. *Biomol. Eng.* **1999**, *16*, 119−125.
(63) Dagda, R. K.; Cherra, S. J., III; Kulich, S. M.; Tandon, A.; Park, D.; Chu, C. T. Loss of PINK1 Function Promotes Mitophagy Through Effects on Oxidative Stress and Mitochondrial Fission. *J. Biol. Chem.* **2009**, *284*, 13843−13855.
(64) Tait, S. W. G.; Green, D. R. Mitochondria and Cell Death: Outer Membrane Permeabilization and Beyond. *Nat. Rev. Mol. Cell Biol.* **2010**, *11*, 621−632.
(65) Kuo, L. J.; Yang, L.-X. γ-H2AX-A Novel Biomarker for DNA Double-Strand Breaks. *In Vivo* **2008**, *22*, 305−310.
(66) Pang, B.; Qiao, X.; Janssen, L.; Velds, A.; Groothuis, T.; Kerkhoven, R.; Nieuwland, M.; Ovaa, H.; Rottenberg, S.; van Tellingen, O.; Janssen, J.; Huijgens, P.; Zwart, W.; Neefjes, J. Drug-Induced Histone Eviction from Open Chromatin Contributes to the Chemotherapeutic Effects of Doxorubicin. *Nat. Commun.* **2013**, *4*, 1908−1920.
(67) Curtin, N. J. DNA Repair Dysregulation from Cancer Driver to Therapeutic Target. *Nat. Rev. Cancer* **2012**, *12*, 801−817.
(68) Theodoropoulos, P. A.; Polioudaki, H.; Kostaki, O.; Derdas, S. P.; Georgoulias, V.; Dargemont, C.; Georgatos, S. D. Taxol Affects Nuclear Lamina and Pore Complex Organization and Inhibits Import of Karyophilic Proteins into the Cell Nucleus. *Cancer Res.* **1999**, *59*, 4625−4633.

DOI: 10.1021/am5090226
ACS Appl. Mater. Interfaces 2015, 7, 7584−7598